POLITECNICO DI MILANO

Facoltà di Ingegneria

Dipartimento di Elettronica, Informazione e Bioingegneria

Master of Science in

Environmental and Land Planning Engineering

Balancing hydropower production and river bed incision

Supervisor:

PROF. RODOLFO SONCINI SESSA

Assistant Supervisor:

ING. SIMONE BIZZI

Master Graduation Thesis by:

SIMONA DENARO

Student Id n. 770356

Academic Year 2012-2013

ACKNOWLEDGMENTS

I would like to express my sincere gratitude to my supervisor Prof. Rodolfo Soncini Sessa for giving me the opportunity to work on this thesis project, his continuous support and motivation guided me in all the time of research and writing.

Besides I would like to thank my assistant supervisor Simone Bizzi for his patience and enthusiasm (sò fiducioso!!), Prof. Francesca Pianosi and Enrico Weber for their precious programming advices and the Ph.D Dario Bernardi for helping me with the model.

To Prof. Andrea Castelletti I am grateful for the chance to participate to the EGU general assembly and for all his advices.

Thanks to Ph.D Quang Dinh for being constantly willing to help, for the Vietnamese food we shared and for always being smiling.

CONTENTS

LIST OF FIGURES

LIST OF TABLES

ACRONYMS

HP Hydro Power

DM Decision Maker

MO Multi-Objective

SO Single-Objective

PB Physical Based

RS Response Surface

RSM Response Surface Method

BCA Best Compromise Alternative

IWRM Integrated Water Resources Management

RSF River Styles Framework

IS Isola Serafini

MEF Minimum Environmental Flow

AIPo Interregional Po Agency

ARPA Regional Environmental Agency

DOE Design Of Experiment

ICOLD International Commission on Large Dams

IEA International Energy Agency

IHA International Hydropower Association

BAU Business As Usual

RBF Radial Basis Function

ANN Artiicial Neural Networks

ABSTRACT

Water management through dams and reservoirs is worldwide necessary to support key human-related activities ranging from hydropower production to water allocation, and flood risk mitigation.

Reservoir operations are commonly planned in order to maximize these objectives. However reservoirs strongly influence river geomorphic processes causing sediment deficit downstream, altering the flow regime, leading, often, to process of river bed incision.

Hydropower plants should be re-operated in such a way to balance energy production and downstream river bed incision, the aim of our research is to investigate the outcomes of this new Multi-Objective (MO) Optimization framework and to assess if the trade-off can be sustainable for the power company.

MO optimization methods of natural complex systems suffer from computational limits, to overcome this shortcoming we propose a framework combining a Parameterization-Simulation-Optimization (PSO) problem together with a global Interactive Response Surface (IRS) approach.

Our case study analyzes the management of Isola Serafini hydropower plant located on the main Po river course. The plant has a major impact on the geomorphic river processes downstream, affecting sediment supply, connectivity and transport capacity.

The new reservoir operations are designed through two different approaches: a feed-forward control law and a feed-forward and feedback control law scheme; the 2-objective PSO problem is solved for the two cases through IRS methodology.

The results provided by both control techniques are finally discussed and critically compared.

Il presente studio analizza le possibilità di gestire il conflitto tra produzione idroelettrica e riduzione del relativo processo di incisione a valle della diga attraverso strategie di controllo ottimale.

Le dighe sono strumenti importanti nella gestione delle acque ed essenziali a diverse attività umane quali la produzione idroelettrica, la minimizzazione del deficit idrico e il controllo delle piene. La gestione di queste strutture è quindi generalmente progettata per soddisfare questi obiettivi; tuttavia la loro azione ha un forte impatto sull'ambiente circostante e in particolare sui processi di geomorfologia fluviale quali erosione, trasporto solido e sedimentazione. La diga infatti rappresenta un'interruzione della naturale continuità tra monte e valle ed è quindi causa di alterazione nei regimi di portata del fiume e disconnessione del naturale trasporto di sedimenti.

Per queste ragioni la legge di controllo che regola i rilasci di una diga andrebbe riprogettata tenendo conto anche degli impatti sulla geomorfologia fluviale attraverso la risoluzione di un problema di ottimizzazione a multi-obiettivo.

Uno dei principali ostacoli all'applicazione di questo approccio è rappresentato dalla difficoltà di combinare i modelli fisicamente distribuiti, necessari a descrivere le dinamiche di geomorfologia fluviale, con le tecniche di ottimizzazione multi-obiettivo i cui costi computazionali diventerebbero insostenibili. Per superare queste limitazioni è qui proposto un approccio risolutivo che affronta il problema di ottimizzazione con l'applicazione del metodo Response Surface (RS).

Il caso di studio preso in esame analizza la gestione dalla centrale idroelettrica ad acqua fluente di Isola Serafini, situata sul corso del fiume Po alle porte di Cremona. Le operazioni di rilascio della diga hanno un considerevole impatto sull'afflusso di sedimenti e sulla capacità di trasporto solido a valle rilevabile in numerosi danni alle infrastrutture e all'ecosistema.

La gestione della diga di Isola Serafini è riprogettata risolvendo il problema a multi-obiettivo tramite il metodo della RS all'interno di due differenti schemi di approccio che esplorano diverse implementazioni della legge di controllo.

1 INTRODUCTION

It is my opinion that the earth is very noble and admirable by reason of the many and different alterations, mutations, and generations which incessantly occur in it..

— Galilei *Dialogue Concerning the Two Chief World Systems*

Recently increased attention was drawn to the evaluation of hydrological adjustments caused by dam operations due to their established effects on the ecosystem and related services. For this reason a growing number of frameworks have been developed for including the evaluation of the geomorphological effects when planning reservoirs operating rules (e.g. Integrated Water Resources Management (IWRM), River Styles Framework (RSF)).

A big challenge in the application of these frameworks is given by the difficulty of embedding fluvial geomorphology into optimal reservoir operation planning: as a matter of fact the models required for evaluating riverbed dynamics are too complex to be implemented into a Multi-Objective (MO) optimization approach.

The present study aims at finding a win-win solution for both hydropower production and riverbed incision applying a surrogate modeling technique to the solution of the MO optimization problem.

The following chapters are organized as follows:

- In the second chapter the impacts deriving from dam operations on the river geomorphology are described together with the current impact management strategies.
- The third chapter is focused on the formulation of the optimization problem and the description of its elements. Moreover the research questions and the posed challenges are explained.
- The forth chapter describes the solution procedure proposed adopted in our research. The RSM is introduced and its procedural steps are explained in detail.
- The fifth chapter is about our case study. First Po river and Isola Serafini system are presented together with the physical based model used to simulate their behavior. Then the attention is focused on the power plant control law and the different frameworks adopted to design a new optimal one.

- In the sixth chapter the general procedural steps described in chapter four are applied to the case study.
- The seventh chapter presents the results.
- In the eight chapter the conclusions are drawn and possible further research is suggested.

Part I

THEORY

2

DAMS AND GEOMORPHOLOGY: INTRODUCTION TO THE PROBLEM

Dams are essential to many key human related activities involving water management. Their purpose ranges from water allocation for irrigation, industrial and domestic supply to Hydro Power (HP) production, flood risk mitigation, land reclamation and recreation. A very general yet eloquent definition of dam was given by ICOLD (1997) [19]: "a barrier or structure across a stream, river or waterway to confine and then control the flow of water".

Dams' history dates back over 5000 years to approximately 3000 BC during Ancient Egyptian Civilization, but it wasn't until the late Middle Ages that they became common in Western Europe. However the majority of dams have only been implemented on waterways around the world since 1950's [29][30] While the peak of dam-building activity in developed country was reached around the '70's, in developing countries, with rapidly growing economies, thousands of dams (especially large ones) have been constructed in the last decades and several more are planned in order to sustain the growing demand of water and energy [18].

However, regardless of their purpose, all dams affect the natural processes of rivers, altering their flow regime and sediment supply; therefore in 1984 Petts describes dams as the greatest point-source of hydrological interference by humans [28]. In natural streams transport of sediment along the river system is continuous, flow rate and sediment transport are linked together and both respond to seasonal peaks. Dams disrupt this longitudinal continuity, trapping sediment upstream and altering the flood peaks and seasonal distribution of flows, causing substantial geomorphological adjustment downstream [21][30].

2.1 IMPACTS

A framework for studying the downstream impacts of dams, through first, second and third order impacts, has been produced by Petts [28] as shown in Figure 2.1. The right-hand side of the first two orders shows the geomorphological aspects of changes on which we are going to focus; the others are associated with ecology. Channel response to dam closure can be very complex and connected to a large series of variables such as the dimension, location and purpose of the dam, the presence of other reservoirs upstream and other anthropic factors including sand mining and land use changes in the catchment.

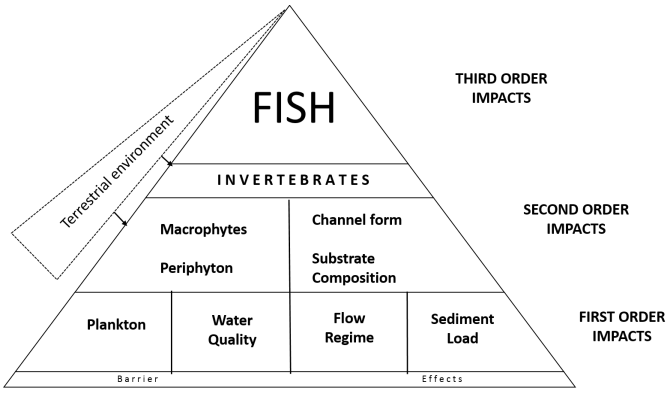

Figure 2.1: A framework for the impacts on impounded rivers (Petts 1984)

Geomorphological adjustments do not occur immediately but a time lag exists between changes to the first-order and those of the second-order and also between phases of adjustment before reaching a new equilibrium. The trajectory of fluvial metamorphosis following dam closure can take a hundred year to be completed [30].

2.1.1 *First-Order Impacts*

As for river morphology, first-order impacts of dam implementation are concerned with changes to the flow regime and sediment load below the dam:

FLOW REGIME Dams affect the hydrological regime downstream "primarily through changes in timing, magnitude and frequency of high and low flows"[23]. Discharge below a dam is generally reduced and flood peaks decrease in magnitude up to 90%, moreover diurnal and seasonal flow patterns may occur due HP operations.

SEDIMENT TRANSPORT The sediment regime is largely affected by dams which can trap almost the entire sediment load delivered by the headwaters upstream. Downstream the water released from the dam is generally clear with highly reduced suspended loads as shown in Figure 2.2; this water is often referred to as *hungry water*, because it has the energy to move sediment and often is the cause for bed incision and banks erosion for years after dam construction and several km away from the structure.

2.1.2 *Second-Order Impacts*

In response to the newly imposed flow and sediment regime the channel attempts to establish a new equilibrium by a complex range of geomorphological adjustment; these can include changes to the channel cross-section and capacity (narrowing or widening of width and

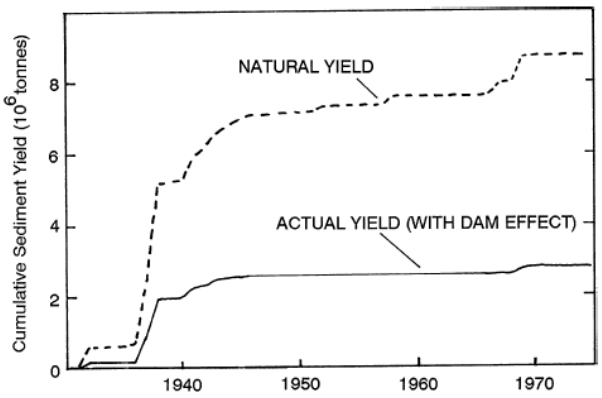

Figure 2.2: Cumulative reduction in suspended sediment supply from the catchment of the San Luis Rey River due to construction of Henshaw Dam [21]

depth), bed coarsening, changes in slope, river patterns (e.g. from braided to single channels) and river bedforms (Figure 2.3 and Figure 2.4). Geomorphological changes are driven by two main processes which can be simplistically presented through a conceptual model known as the Lanes Balance; as summarized by Grant [17] it states that "if the transport capacity exceeds the available supply, a sediment deficit exists and the channel can be expected to evacuate sediment from its bed and/or banks. If the transport capacity is less than the available sediment supply, then the channel can be expected to accumulate sediment":

INCISION AND EROSION As seen inSection 2.1.1 the *hungry water* discharged by the dam has excess energy due to low sediment load. The river aims to satisfy the required sediment load initially and primarily by degrading the channel bed (riverbed incision) and then eroding the banks. Both bed incision and bank erosion can extend over hundreds of kilometers. Degradation reduces the channel slope and can lead to changes in particle size of the bed material as gravels and finer materials are winnowed from the bed and transported downstream heading to the exposure of bedrock or more resistant layers; this armor layer may continue to coarsen until the material is no longer capable of being moved by the reservoir releases, thereby limiting the ultimate depth of incision.

AGGRADATION AND DEPOSITION Although incision may be the initial adjustment below dams, aggradation is likely to occur further downstream. Sources of sediment downstream include material previously eroded by the clear water and from unregulated tributaries. This can induce riparian vegetation growth and encroachment along the channel banks. However, in some

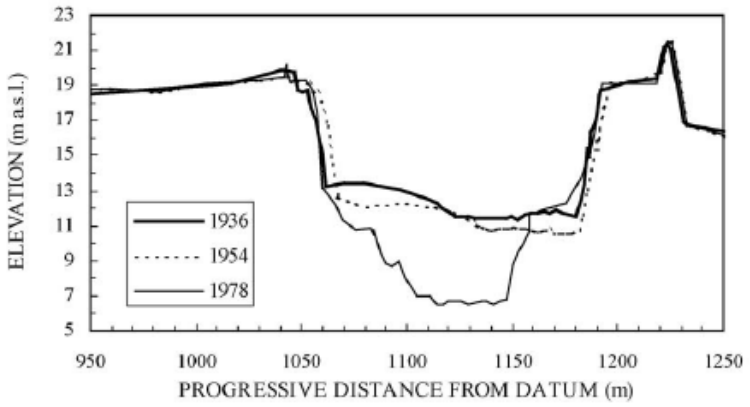

Figure 2.3: Channel incision along the Arno River in the Lower Valdarno–Pisa Plain reach: example of typical change in cross section, with limited bed lowering from 1936 to 1954, and intense incision from 1954 to 1978. Total bed level lowering from 1844 to 1978 was 6.3 m [44].

cases, deposition never occurs due to low sediment load, and the suspended sediment reaches the sea.

2.1.3 *Impacts on the Ecology*

Dams have a significant impact on freshwater ecosystems, it is estimated that dams have fragmented 60% of the rivers around the globe [25]. Altering flow and thermal regime and the water chemistry, dams affect biota and biodiversity producing first to third-order impacts:

- **primary production:** phytoplankton, periphyton and macrophytes which form the base of the food-web are very sensible to the changes in ecosystem conditions produced by dams.
- **molluscs:** although widely distributed, many freshwater mollusc species only occur over a relatively narrow range of habitat conditions. Consequently, dam construction can cause stress and ultimately undermine species survival or, conversely, it may provide opportunities for non-native species [1].
- **fish:** blockage of migration routes causes marked changes in fish populations both upstream and downstream of dams, changes in flow regime, physio-chemical conditions, primary production and channel morphology generally have an adverse effect

1 The number of native species remaining in an ecosystem is an important indicator of biodiversity [33].

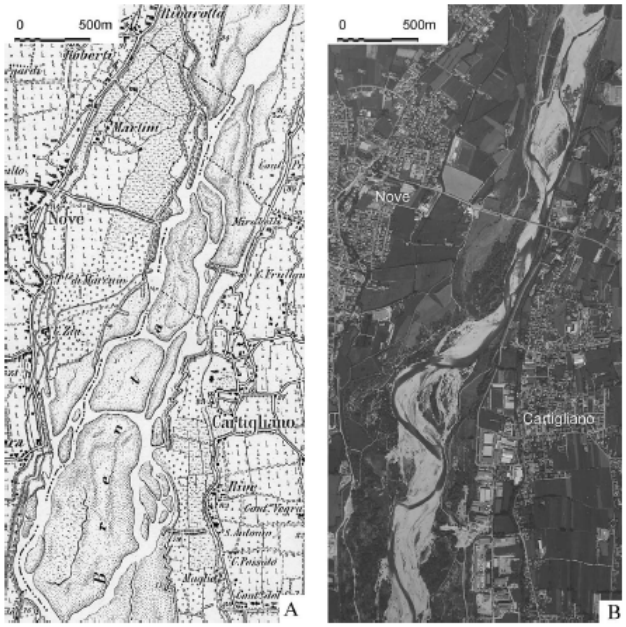

Figure 2.4: Channel narrowing along the Brenta River: (A) topographic map (I.G.M.) of 1887; (B) aerial photograph of 1999. Besides narrowing, decrease in intensity of braiding, increase in channel sinuosity and change in channel pattern (from braided to wandering) have taken place during the last century [44].

Figure 2.5: Spawning salmon in the Sacramento-San Joaquin River watershed

on the majority of native species. Moreover bed coarsening can threaten the success of spawning by salmonids (salmon and trout), which use freshwater gravels to incubate their eggs (Figure 2.5).

- **birds and mammals:** The creation of reservoirs can have both positive and negative effects for aquatic and terrestrial species: in tropical areas flooding results in habitat loss and species extinction; on the contrary, in arid climates, reservoirs provide a permanent water resource that can benefit many species. In any case, the most negative effect of river regulations on mammals and birds is the disruption of the seasonal flood regime along the river: in the long term this can alter vegetation communities that may be important for a wide range of species.

2.1.4 *Other secondary impacts*

Other secondary impacts include effects on infrastructure stability and functioning: incision undermines bridges (Figure 2.6); riverbed lowering causes malfunction of facilities such as navigation locks affecting both fishing and tourism; irrigation devices like sluice gates become unusable during low flow periods; coastal erosion and the previously mentioned alteration of important ecological processes have impacts on water quality and biodiversity.

2.2 CURRENT IMPACT MANAGEMENT STRATEGIES

2.2.1 *Environmental protection*

In many countries increased environmental awareness motivate the integration of environmental protection measures in dam projects. This tendency has been stimulated by different factors:

- Policies and legislation. The need for more sustainable water related processes is translated at the political levels into international conventions (e.g. Rio Declaration on Environment and Development, the Convention on Biological Diversity, the Convention on Wetlands of International Importance ...) and international and national policies (e.g. the European Union Water Framework Directive, the South African Water Law, the US National Environmental Policy Acts). These do not relate specifically to dams, nevertheless they provide the right context and framework for environmental protection measures in dam projects.
- Conditions of financial support. Many investment institution, such as the World Bank or the European Union, requires specific policies that promote environmental protection measures

(a) *Arno river*.

(b) *Rhine river*.

Figure 2.6: Effects on infrastructures stability: bridges with exposed piles due to riverbed incision [44][36].

in large dams projects. However, financial institution ability to enforce the implementation of effective environmental programs is limited.

- Practitioner codes of conduct. The International Commission on Large Dams (ICOLD), the International Energy Agency (IEA) and the International Hydropower Association (IHA) have developed guidelines that encourage the highest standards in the planning and implementation of large dam projects. These guidelines include ways to protect the environment. At present there is no way to force companies into following these codes of conduct, however the concern for negative publicity is a motivation for increasing transpositions.

For new dams three types of measures can be identified:

AVOIDANCE MEASURES That is alternative to dam construction.

MITIGATION MEASURES To reduce the undesirable effects of a dam by modification of its structure or operation, or through changes to the management of the catchment within which the dam is situated. This approach is the most used for ameliorating the negative effects of dams and includes several technical interventions (Table 2.1).

COMPENSATION MEASURES Effects that can neither be avoided nor sufficiently mitigated can be compensated. Compensation measures include ecologic areas preservation and rehabilitation of previously disturbed land present around the the reservoir.

For existing dams, amelioration measures also include restoration, which comprises attempts to return ecosystems to an approximation of pre-disturbance conditions. Within this context, dam decommissioning is increasingly being considered as a viable option [25].

2.2.2 *Structure rehabilitation*

Reconstruction strategies can be implemented in order to restore infrastructure functionality and stability. These measures can range from small to considerable interventions: diaphragm walls can be included in the foundations to avoid piping phenomena; the gaps present under the sills can be filled with grout so that the structure can resume its contact to the ground; baffle blocks upstream can dissipate a significant amount of energy; ground elevation at toe can be restore with heavy mattresses and protected by means of concrete cages [26].

The solution proposed in our research wants to confront the problem of environmental impacts of dams within a totally new perspective: impact control is not sent to a secondary phase of management

ISSUE	MITIGATION MEASURES
Flow regime	Managed flow releases
Thermal regime	Multi-level outlet works
Water quality	Outlet works aeration
	Multi-level outlet works
	Turbine venting
Sedimentation	Addition of sediments to rivers
	Managed flow releases
	Shoreline stabilisation
Weeds/algal blooms	Mechanical cutting
	Chemical control
	Biological control
	Flushing
Fish	Freshets to stimulate fish migration
	Improved design of turbine, spillways and overflows
	Fish passes
	Artificial spawning areas
	Hatcheries and fish stocking
Terrestrial wildlife	Managed flow releases

Table 2.1: Technical interventions for mitigating the impacts of dams on ecosystems [25]

design but is imbedded into the optimal planning of the dam operations. For this reason we believe our approach is different from all current impact management strategies.

3

PROBLEM FORMULATION

Relationship between dams operation and geomorphological effects on the catchment has been extensively observed and confirmed by several studies in the last decades [3][4][15][17][18][21][29][30][33][35]. Nevertheless, when planning operational rules only the fulfillment of the main purpose (or purposes)[1] for which the structure was built is considered and no or little attention is given to the impacts these operations are going to have on the river morphology. A new and better policy should also include riverbed incision abatement among its objectives.

The aim of an *optimization problem* is to find the *Pareto-efficient* alternatives among the feasible ones. Pareto efficiency, is a concept introduced by the Italian economist Vilfredo Pareto in the 19^{th} century; it represents a state where resources are allocated in the most efficient manner. Pareto efficiency is obtained when a distribution strategy exists where one objective's performance cannot be improved without worsening another objective's conditions. Given a set of alternatives and a way of valuing them, the Pareto set (or Pareto front) is the set of choices that are Pareto-efficient. The *objectives* express *stakeholders*[2] point of view. The *Decisor Maker* (DM) holds the political authority to choose which alternative will become effective among the Pareto-efficient ones. In general, his goal is to find the Best Compromise Alternative (BCA) [7][13].

Involving a new objective, such as riverbed incision abatement, into the planning of the optimal operation rule can have many different outcomes; it entails the scope widening in a new different framework. If the old and new objectives are not conflicting nothing really has to change, the old policy will do. On the contrary, if there is a conflict, a wide range of different trade-offs[3] can occur: we could figure out that a slight little change on the old policy could have a large positive effect on our new objective and this could lead to a shared new alternative; however incompatible objectives could cause unbearable

1 some large dams can be multi-purpose (e.g. HP and water allocation) and their operation can already be planned solving a MO problem which is suitable for striking a balance between conflicting objectives

2 That is every person, institution or organization possibly affected by the outcomes of a certain alternative

3 When choices are made (collectively or by an individual) to accept having less of one thing in order to get more of something else, the results are called trade-offs.

trade-offs and it would be impossible to find a balanced new policy.

For a generic dam, at the time t, water release decision u_t is determined by the control law m_t which depends on the information I_t available at the time t and a vector $\mathbf{p}$ of parameters:

$$u_t = m_t(I_t, \mathbf{p}) \tag{3.1}$$

The parameter vector $\mathbf{p} = [\theta_1, \theta_2, \dots \theta_n]$ defines a specific control law in the class of functions $m_t(I_t, \cdot)$. The vector $\mathbf{p}$ is time invariant and can be designed through an optimization design problem.

3.1 THE OPTIMIZATION PROBLEM

Our optimization problem aims at finding the parameter vectors $\mathbf{p}$ that, given a class of control laws, are optimal in Pareto sense both for hydropower production and riverbed incision.

They have to be looked for within feasible alternative set $\mathcal{P} \subseteq \mathcal{R}^n$ which includes all the combinations of parameters that are physically and legally possible.

To solve an optimization problem a mathematical model is needed in order to evaluate all feasible alternatives in terms of objectives performances.

Therefore to quantify the satisfaction rate of each objective we define a set of indicators $J^1(\cdot), \dots, J^m(\cdot)$ that condense the information contained in the model output via time and space aggregation of the trajectories of the system variables [42].

The MO optimization problem assumes the form:

$$\min_{\mathbf{p}} \mathbf{J}\left(\mathbf{x}_0^h, \mathbf{a}_0^{h-1}\right) = \min_{\mathbf{p}} \left[J^1\left(\mathbf{x}_0^h, \mathbf{a}_0^{h-1}\right), \ldots, J^m\left(\mathbf{x}_0^h, \mathbf{a}_0^{h-1}\right)\right] \quad (3.2a)$$

subject to

$$u_t = m_t(I_t, \mathbf{p}) \qquad t = 0, 1, \ldots, h-1 \quad (3.2b)$$

$$x_{t+1} = f_t(x_t, u_t, a_{t+1}) \qquad t = 0, 1, \ldots, h-1 \quad (3.2c)$$

$$\mathbf{p} \in \mathcal{P} \quad (3.2d)$$

$$I_t \quad \text{to be chosen} \qquad t = 0, 1, \ldots, h-1 \quad (3.2e)$$

$$\mathbf{a}_0^{h-1} \quad \text{scenario} \quad (3.2f)$$

$$x_0 = \bar{x}_0 \quad (3.2g)$$

Where J^i (i=1,...,m) are the m objectives to be minimized (or maximized).

x_{t+1} represents the model state variables whose trajectory is determined by the *state transition function* f_t and depends on the previous state x_t, on the water release decision u_t and on the inflow a_{t+1} given by the scenario $\mathbf{a}_0^{h-1}$.

In turn the water release decision u_t is defined by the control law $m_t(\cdot)$ which is determined by the parameter vector $\mathbf{p}$ and the time-variant information I_t.

All vectors $\mathbf{p}$ need to be within the feasible set $\mathcal{P}$.

3.2 THE CONTROL LAW

Our research aims at finding a new control law which is optimal in Pareto sense for both hydropower production and riverbed incision.

Control laws can differ in shape, the control mechanism and the parametrization.

In our research we focused on two particular types of control law: the *feed-forward* and the *feedback* control law.

- The *feed-forward* control (Figure 3.1), also called anticipative control, takes corrective action in order to anticipate the effects of the measured disturbances a_t. For a dam management this means that at each time t the inflow a_t generated by the upstream catchment is measured and a certain water release decision u_t is determined according to the control law which, in turn, is defined by the parameter vector $\mathbf{p}$.

- The *feedback* control obtains data at the process output and uses this information to achieve the desired result: the variable being controlled is measured and compared with a target value; then the *feedback* control law manipulates the control u_t in order to

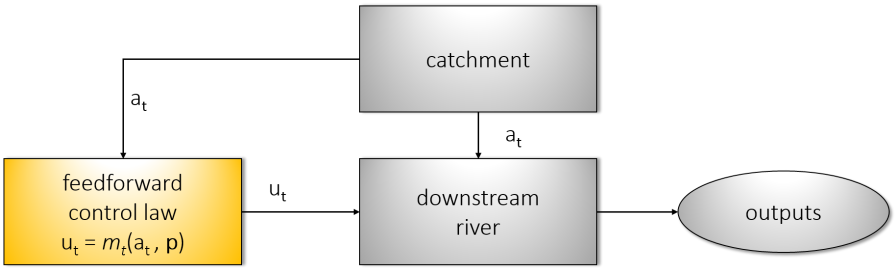

Figure 3.1: Feed-forward control scheme

minimize the difference between the actual and desired value of the output at the next time step.

A dam regulator could combine together both *feed-forward* and *feedback* control (Figure 3.2): the system output generated by a certain *feed-forward* control law could be used to determine a new parameter vector **p** through a *feedback* control law. This new parameter vector will modify the *feed-forward* control law at the next time step. The procedure could be repeated iteratively.

3.3 THE MODEL

To quantify the effects each alternative would have when implemented, a model is needed to describe the cause-and-effect relationships in the system. These relationships make up the state transition function (3.2c)

Riverbed evolution dynamics require medium/long period simulation runs of a spatially distributed model in order to be determined. This requires very high computational costs.

The model adopted in the present case study is a physical based one-dimensional model, able to represent 1D flows with mobile bed in natural channels of complex geometry. To perform a 10 year simulation run using the power of an average processor, this model requires 3.5 days.

Therefore we clearly can assess that a model simulating river geomorphology cannot be applied to evaluate a great number of alternatives for decision making.

3.4 CHALLENGES

Geomorphic processes are not negligible when planning reservoirs optimal control, this is true both for the undeniable impacts of dams operation whose negative effects have to be controlled, and for the scenario models themselves, whose outcomes are clearly influenced by geomorphological adjustments. Nevertheless there are not yet example, in our knowledge, that tried to couple together riverbed incision

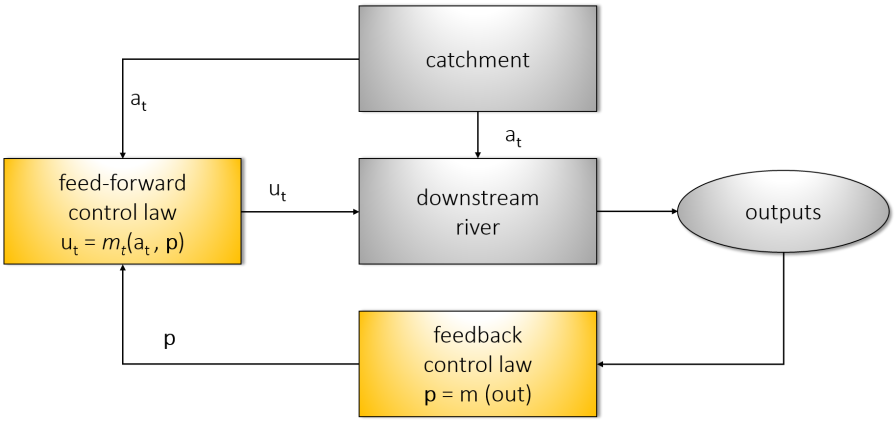

Figure 3.2: Feed-forward and feedback regulator scheme

abatement and optimal planning; one explanation for this behavior is the difficulty of simulating the complexity of river geomorphic response.

Nowadays, thanks to computing power improvements, it is possible to run a 1D or 2D model able to simulate both hydrodynamic and riverbed evolution in space and time, these kind of models would be suitable for estimating the river morphological response to dam closure, however their computational costs are very high.

As seen in the previous section, MO optimization methods need to evaluate a very large number of different alternatives in order to identify the Pareto-efficient ones and find the BCA. This procedure would require a prohibitively large amount of simulations of the PB model thus making the optimization practically unfeasible.

3.5 RESEARCH QUESTIONS

This research wants to investigate the possibility of re-operating HP plants in such a way to balance energy production and downstream riverbed incision.

The solution of this problem poses several challenges due to the difficulty of embedding fluvial geomorphology into optimal reservoir operation planning as (Section 3.4).

We will focus on a real case study in order to first understand the best way to design a new policy and to analyze the trade-offs between the two objectives using a surrogate modeling technique called Response Surface Method RSM (Section 4.1).

At the end it will be possible to state whether a new, balanced operation rule of the dam would be sustainable for the power company.

4

SOLUTION PROCEDURE

In Chapter 3 the main challenge of embedding fluvial geomorphology into optimal reservoir operation planning was expressed: optimization techniques require a large number of alternatives evaluation achieved by means of a model reproducing the system behavior.

To simulate natural processes, such as riverbed evolution, a spatially distributed model is needed. For this kind of model a large number of evaluations is computationally unfeasible.
To overcome this limitation the computationally-onerous Physical Based (PB) model can be replaced by a *surrogate model*.

Surrogate modeling represents a second level of abstraction since it provides a cheaper-to-run model of the original model, for this reason they are also referred to as *metamodels*.

A wide variety of surrogate models have been developed over the past decades and their use is becoming more and more popular within the water resources community [34].

Response Surface (RS) surrogates are a particular family of *metamodels*, one procedure for performing this reduction is called the Response Surface Method (RSM).

4.1 THE RESPONSE SURFACE METHOD

The Response Surface Method (RSM) was first proposed by Box and Wilson in 1951 [2] and consists in the approximation of a multi-dimensional function, called Response Surface (RS). Optimization problems like 3.2 aim at minimizing (or maximizing) the *Response Surface* function $f(\mathbf{p})$:

$$\min_{\mathbf{p}\in\mathcal{P}} \mathbf{J} = f(\mathbf{p}) \tag{4.1}$$

Where $f(\cdot)$ is a function $f : \mathcal{R}^n \to \mathcal{R}^m$ that includes all relations between elements in $\mathbf{p}$ and $\mathbf{J}$ mediated by the physical based model (which means it contains the information given by the state transition equation 3.2c). In other words, the RS maps the n design parameters into the m-dimensional objective space.

The Response Surface $f(\cdot)$ (which is typically a nonlinear hyperplane) gives the performance in terms of indicators of each combination of parameters according to the PB model. This is the kind of information we need in order to draw the Pareto front. However this

surface remains unknown because of already mentioned computational limitations of the model. However an approximation $\hat{f}(\cdot)$ can be identified and on its basis we can solve the optimization problem.

RSM uses a low order regression model in place of the original one in order to approximate the RS; with only a limited number of simulations and a large, complex alternatives space it's important to define a *procedure* in order to maximize the information produced and effectively allocate the experiment runs. Castelletti et al [6][9] first proposed an iterative and interactive a-posteriori procedure consisting of two phases:

LEARNING during this phase a sample of input (the engineering alternative to be evaluated) and output (the performance of the alternative in terms of indicators) pairs is generated through a set of suitably designed simulation runs of the PB model. The sample is then used to identify an approximation of the RS

PLANNING during this phase an approximated Pareto front and the associated set of Pareto-efficient alternatives are obtained by using the current RS approximation. The Decision Maker (DM) selects one or more *interesting* alternatives.

The two phases are then performed iteratively improving the effectiveness of the approach; in fact, while the learning phase is limited by the number of simulation runs that can be performed, the planning phase can exploit the optimization results for increasing the sampling in those region of the decision space which are more *interesting* from the DM point of view. The iteration continues until a termination test is fulfilled.

Two approaches are possible for the approximation of the RS (Figure 4.1): a *global approach*, where the RS is identified over the whole feasible alternatives space, and a *local* one, where the RS is only approximated in the neighborhood of the current BCA. In the former case we are conducting a proper optimization among the alternatives, in the latter one we are just searching for an improvement of the current best solution available.

4.2 STATE OF ART

Many different surrogate modeling methods have been applied within optimization frameworks of a wide range of environmental problems [34]. The RSM was invented over 60 years ago and was widely implemented both for Single-Objective (SO) and MO optimization problems[20]. Castelletti et al [6][9] first proposed to include it into a heuristic interactive procedure in order to overcome computational limitations of environmental systems optimal control problems; both local and global approach were adopted and compared [11].

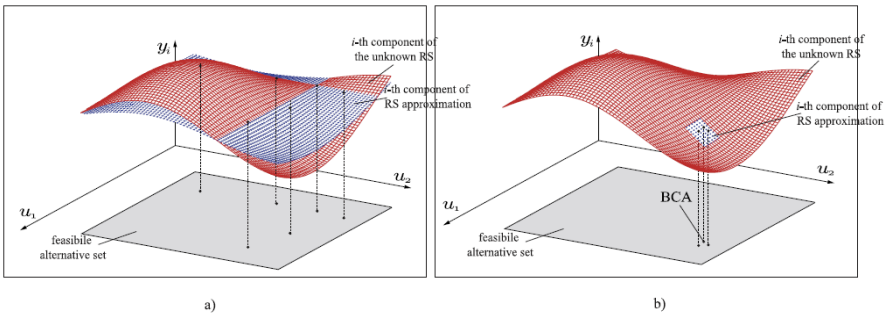

Figure 4.1: (a) Global and (b) local approximation of the i-th component of the unknown RS.In both the panels, the red surface is the unknown surface; the blue surface is the approximated one [11].

Today we assist at the increasing concern for environmental protection and demand for sustainable development; the adoption of paradigm and procedure like IWRM and RSF demonstrates that a stronger combination of physical processes complexity and optimal control of environmental structure is necessary and possible. We already encountered real cases in which water quality was considered when designing reservoir operation rules [47]; nevertheless dams regulation effects on fluvial morphology downstream was never implemented into MO optimization of the operation rules.

Coupling together the advances in understanding physical and ecological processes of fluvial systems and the theory of surrogate modelling a new, more conscious framework for water management could be possible.

4.3 THE PROCEDURE

Here the global RSM procedure is described in detail. This procedure will be adopted in our research to solve a MO optimization problem (3.2).

The *Learning and Planning* procedure consists of four iterative steps plus an initialization and termination test (Figure 4.2).

The four steps at the k-th iteration are as follows:

4.3.1 *Initialization*

The initialization step consists in the selection of the first N_0 input vectors $\mathbf{p}^1, \mathbf{p}^2, \cdots, \mathbf{p}^{N_0} \in \mathcal{P}$ to be simulated at the first iteration (k=0). For effectively sampling the decision space a Design Of Experiment (DOE) can be employed. DOE can be operated in many different ways: using statistical techniques or by means of physical consideration and a-priori knowledge. In any case the sampling points distribution must be homogeneous in the alternative set. The value of N_0 depends on the specific computational burden of the model, the available compu-

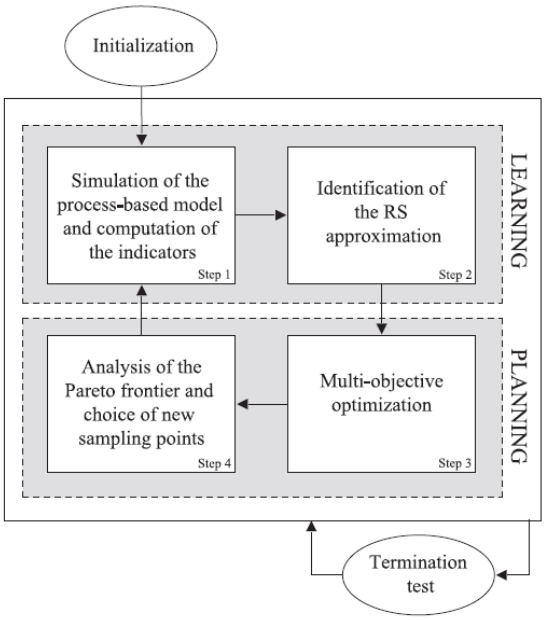

Figure 4.2: The iterative learning and planning procedure based on RS approximation

tational power and the time at hand. The goal is to find a compromise between computational burden and results precision.

4.3.2 *Step 1: Simulation of the PB model and computation of the indicators*

N_k simulations of the PB model are run using N_k different alternatives. Based on the model outputs the corresponding indicator vectors J are computed.

4.3.3 *Step 2: Response Surface identification*

The simulated data pairs (**p**, **J**) generated up to the k-th iteration are used to identify the RS approximation $\hat{f}(\cdot)$. Many different methods exist to identify the approximated RS: they range from simple polynomial interpolation to splines and neural networks. In Section 6.4 the methods used in our research will be described in detail.

4.3.4 *Step 3: MO optimization problem*

In order to find Pareto-efficient solutions among the RS the following problem is solved:

$$\min_{\mathbf{p}\in\mathcal{P}} \mathbf{J} = \hat{f}^{k}(\mathbf{p}) \tag{4.2}$$

The $\hat{f}^{k}(\cdot)$ can be used for a large number of evaluations since its computational cost is by far lower than the PB model one. If the feasible alternatives set $\mathcal{P}$ is finite and reasonably small, one can solve the problem for each alternative $\mathbf{p}$ and obtain a complete Pareto-front. Otherwise, if the feasible set is infinite or too large, the problem is solved for a evenly distributed set of alternatives. In the latter case an approximation of the Pareto front is obtained and the paretian solutions are suboptimal.

4.3.5 *Step 4: Pareto front analysis and selection of* interesting *alternatives*

The Pareto front obtained at step 3 is analyzed and *interesting* points in the objective space are identified. The associated points in the decision space constitute the new alternatives to be simulated at step 1 of the next iteration. This selection can be operated by an expert (e.g. the DM himself) or through an automatic ranking criterion.

Once an *interesting* point $\hat{\mathbf{J}}$ has been chosen, the alternative $\mathbf{p}$ that generated it has to be derived. This is possible by inverting the RS, which can be performed in two ways:

NUMERICAL INVERSION The RS is analytically inverted, which means the problem $\hat{f}^{k}(\mathbf{p}) = \hat{\mathbf{J}}$ is solved. However, this approach is unfeasible when $n < m$. this approach is not possible.

SINGLE OBJECTIVE OPTIMIZATION When $n < m$ the decision $\widetilde{\mathbf{p}}$ that generated the the point $\widetilde{\mathbf{J}}$ can be found solving a minimum distance problem:

$$\min_{\mathbf{p}\in\mathcal{P}} \left\| \hat{f}^{k}(\mathbf{p}) - \hat{\mathbf{J}} \right\| \tag{4.3}$$

Where $\|\cdot\|$ is the Chebyshev norm.

4.3.6 *Termination test*

The termination test can be performed starting from the second iteration (k=2) through two different criteria: one possibility is to stop the procedure when the RS converges, that is when the distance between

the $f^{k}(\cdot)$ and $f^{k-1}(\cdot)$ at two consecutive iterations is below a given threshold. However, this method is only able to check the convergence of the RS approximation and not the accuracy of the estimate of the RS $f(\cdot)$. Alternatively the procedure can be terminated when the average distance between outputs simulated by the PB model and the ones computed through RS approximation is below a given threshold.

Part II

PRACTICE

5 THE CASE STUDY

5.1 PO RIVER AND ISOLA SERAFINI POWER PLANT

Figure 5.1: Po springs

The Po river is a northern Italian river running eastwards from its springs in the Cottian Alps (Figure 5.1) to a wide branched delta projecting into the Adriatic Sea near Venice. It flows for 652 km through the Padan plain reaching many important Italian cities, such as Torino, Piacenza and Ferrara. It's the longest Italian river and its drainage area of over 71 000 km² makes it the biggest Italian catchment. Padan plain is one of the most economically active area in Italy (Figure 5.2) holding over a third of the total agricultural and industrial sectors and half of the Italian livestock resources. For its strategic location and morphological features Po river is known as the main Italian river [32].

Figure 5.2: A typical view over the Padan plain

River Po environmental services are extensively exploited for a wide range of purposes ranging from water allocation for farming lands, industrial and domestic use, sand mining for construction materials and HP production. Isola Serafini (IS), one of the biggest fluvial islands of the river, houses one of the most important structure in the Po river with the main purpose of HP production: the IS run-of-the-river power plant (Figure 5.3).

5.1.1 *Isola Serafini power plant*

Located in the Municipality of Monticelli d'Ongina (PC), 20 km westbound Cremona, Isola Serafini, with its 350 m wide dam, is the largest run-of-the-river power plant in Italy (Figure 5.4).

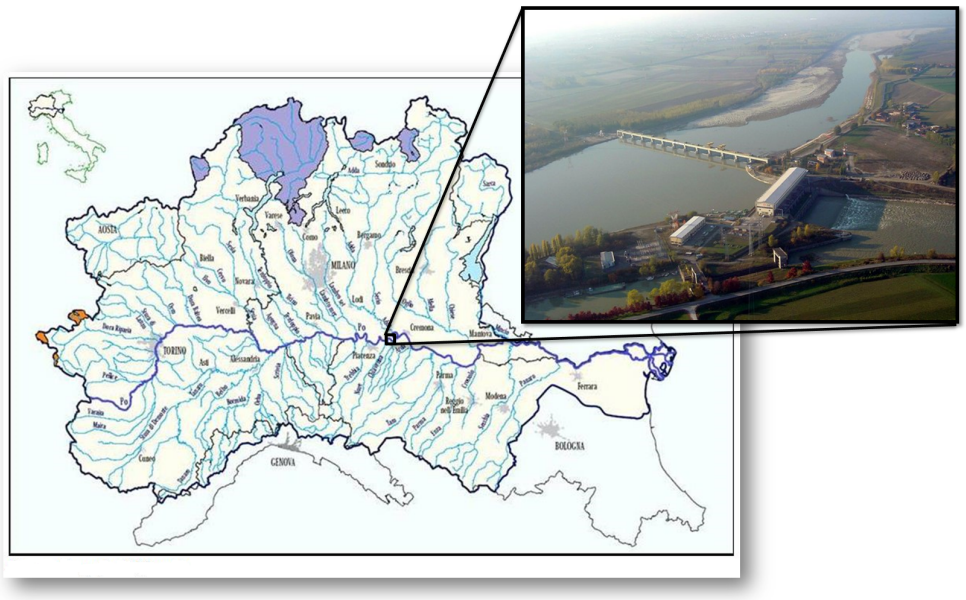

Figure 5.3: Isola Serafini location in the Po valley

Figure 5.4: Outside and inside view of IS power station with its four Kaplan turbines

Managed by the Italian energy agency ENEL, was completed in 1962 and has a total installed power capacity of 80 MW and a mean annual hydroelectric production of 480 GWh.

Part of the Po discharge is conveyed to the power plant up to a maximum diverted flow of 1000 m^3/s and shared among four Kaplan vertical turbines of 12.5 MW each; the diverted flow joins again the Po river about 12 km downstream the gate after a large meander through an artificial channel. The dam is formed by eleven openings equipped with vertical lift gates on trolleys; six gates can work also as sharp-crested weirs. Hydraulic head can vary between 7.5 a 3.5 m according to downstream conditions[1] [26].

5.1.2 *Po current problems*

Due to intense sediment mining, the middle course of Po underwent a strong river bed degradation process in the years from 1950 to 2000 (Figure 5.5), characterized by severe rates until 1980s; recently, stricter regulations on instream sediment mining have partially stopped this activity.

Along with sediment mining, also low water training for navigation purposes and the presence of dams in the upper part of the Po basin affect the overall sediment balance along the middle course.

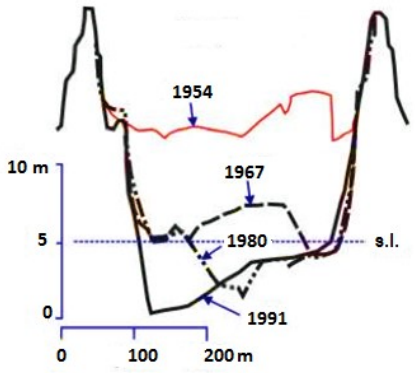

Figure 5.5: Po river section showing riverbed incision in the last decades [45]

Besides, the presence of Isola Serafini HP plant plays an important role since its building in the 60's. IS barrage is trapping sediment upstream, causing an abrupt decrease in sediment supply downstream and affects the hydrological regime reducing the transport capacity of the river in the meander downstream. Riverbed incision downstream of IS dam is well documented by the minimum water stages per year recorded at Cremona station, decreasing by more than 4 m from 1950 to 2000 (Figure 5.6).

All these effects have an impact on infrastructure stability, navigation locks operation and ecological processes of the freshwater environment (Figure 5.7) .

1 Upstream conditions can be controlled instead; as a matter of fact, when the HP station is working, the upstream level is kept constant at 41 m

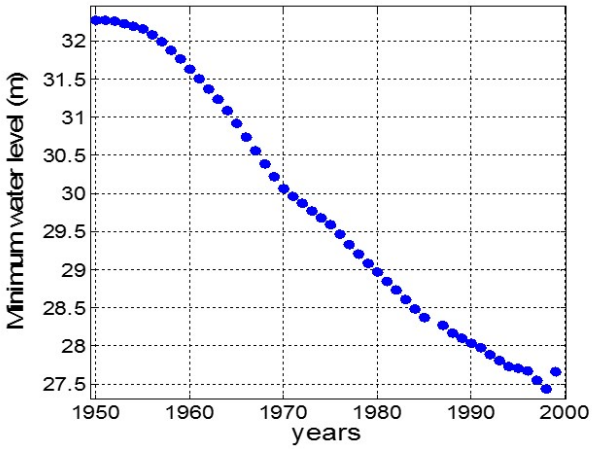

Figure 5.6: Minimum water stages per year recorded at Cremona station from 1950 to 2000

(a) *Undermined bridge.*

(b) *IS navigation lock made useless by riverbed incision.*

(c) *Cranes replace navigation locks for boats raising/lowering operation.*

Figure 5.7: Po riverbed incision effects on infrastructures

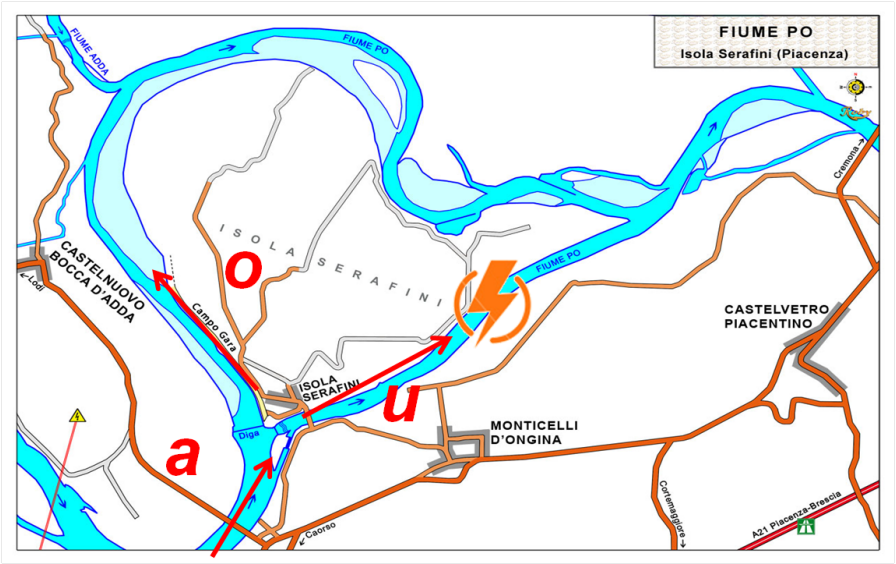

Figure 5.8: Isola Serafini system description: the incoming discharge a is partially diverted to the turbines (u) and partially to the meander (**o**)

5.1.3 *Isola Serafini system*

IS system is described in Figure 5.8: the power plant is placed on the river island formed between two channels, a natural meandering one and the artificial tailrace canal; the gate partially diverts the incoming discharge a to the turbines (u) and partially to the meander (o) where a Minimum Environmental Flow (MEF) is required. The two flows merge again 12 km downstream the gate.

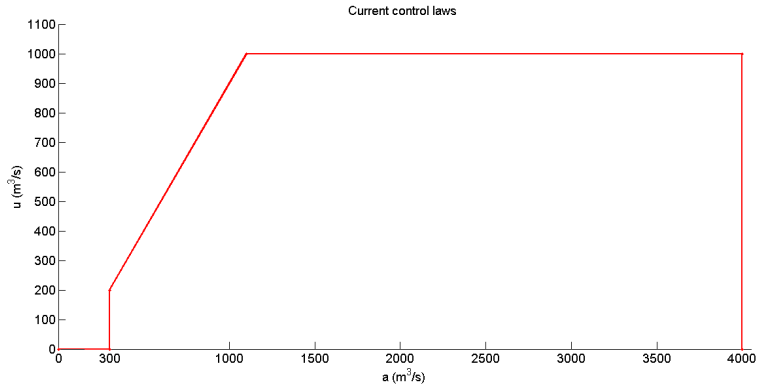

Figure 5.9: Isola Serafini current *feed-forward control* control law: the discharge a is measured and the corresponding water release decision u is applied

5.1.3.1 *The current control law*

The current control law of IS (Figure 5.9) is a piecewise linear function based on a *feed-forward control*.

At each time t the decision variable u is determined by the related discharge a according to the control law.

The control law is subject to physical and legal constraints: since a MEF of 100 m^3/s is required through the meander and the minimum flow through the power station is 200 m^3/s , when the incoming discharge a is not greater than 300 m^3/s, the power station is not working.

When a is greater than 300 m^3/s, all flow exceeding MEF is diverted to the turbines until a maximum permitted of 1000 m^3/s. Therefore, when the inflow a is above 1100 m^3/s the power station can work at his maximum and all incoming flow exceeding 1000 m^3/s passes throughout the gate and flows into the meander.

The station can work until the total discharge reaches approximately 4000 m^3/s; above this threshold, the head jump across the gate becomes too low for electricity generation. In addition, to avoid flooding risk, the turbines are switched off and the gate must be completely open to let the flood pass through.

When incoming flow a is lower than 4000 m^3/s the water level in the reservoir is kept constant at 41 m to maximize the head jump and the energy production.

5.2 THE PHYSICAL BASED MODEL

A physical based one-dimensional model, able to represent 1D flows with mobile bed in natural channels of complex geometry was used.

The model is based on a set of three differential equations, stating mass and momentum conservation for the liquid phase (5.1 and 5.2) and mass conservation of the solid phase (5.3) along the main stream direction [41].

$$\frac{\partial A}{\partial t} + \frac{\partial Q}{\partial l} = q \tag{5.1}$$

$$\frac{\partial Q}{\partial x} + \frac{\partial}{\partial x}\left(\frac{Q^2}{A + gI_1}\right) = g\frac{\partial I_1}{\partial x}\bigg|_w - gAS_f \tag{5.2}$$

$$(1-p)\frac{\partial A_b}{\partial t} + \frac{\partial Q_s}{\partial x} = q_s \tag{5.3}$$

Where t is the time, l is the longitudinal stream coordinate, A is the cross-section wetted area, Q is the liquid discharge, g is the gravity acceleration, $I1$ is the static moment of the wetted area A with respect

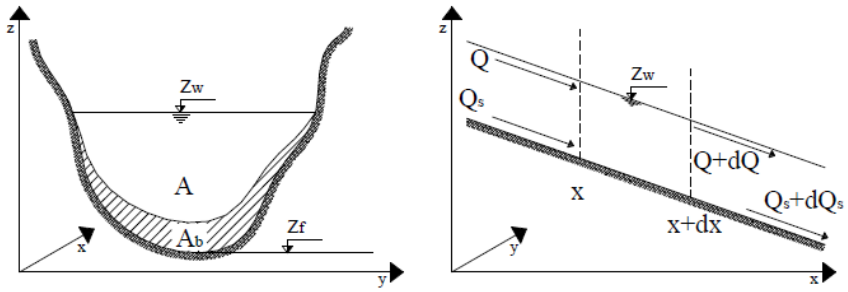

Figure 5.10: Channel section scheme and variables description

to the water surface, S_f is the friction slope, A_b is the sediment volume per unit length of the stream subject to erosion or deposition ("sediment area"), Q_s is the solid discharge, p is the bed porosity, q and q_s are the liquid and solid lateral inflows (or outflows) per unit length, respectively (Figure 5.10). The first term in the right-hand side of equation (5.2) represents the variation of the static moment $I1$ along the l coordinate at a constant water level w.

For the slope friction, the common Manning formula has been used:

$$S_f = \frac{n^2 Q^2}{A^2 R^{4/3}} \tag{5.4}$$

For solid lateral flows q_s the Engelund-Hansen formula is adopted:

$$q_s = 0.05 \cdot \rho_s g U^2 \sqrt{\frac{d_s}{g\,(s-1)}} \cdot \left(\frac{T_0}{\rho g\,(s-1)}\right)^{3/2} \tag{5.5}$$

Where q_s is the solid discharge per unit width; ρ and ρ_s are the densities of water and sediments respectively; s is the relative density ρ_s/ρ; d_s is the sediments representative diameter; U is the water average velocity; T_0 is the bed shear stress.

The solution of the balance equations 5.1 5.2 and 5.3, obtained through McCormack's finite difference explicit integration scheme, updates the values of wetted area A, liquid discharge Q and sediment area A_b at each time step. This value has to be converted into a bed elevation variation, Δ_s for every wetted point of the cross section. Since the model is one-dimensional this conversion has to be done under some kind of assumption: here we assume that this variation Δ_s is proportional to bed shear stress; this criteria is supposed to be the best choice for representing real riverbed evolution [27].

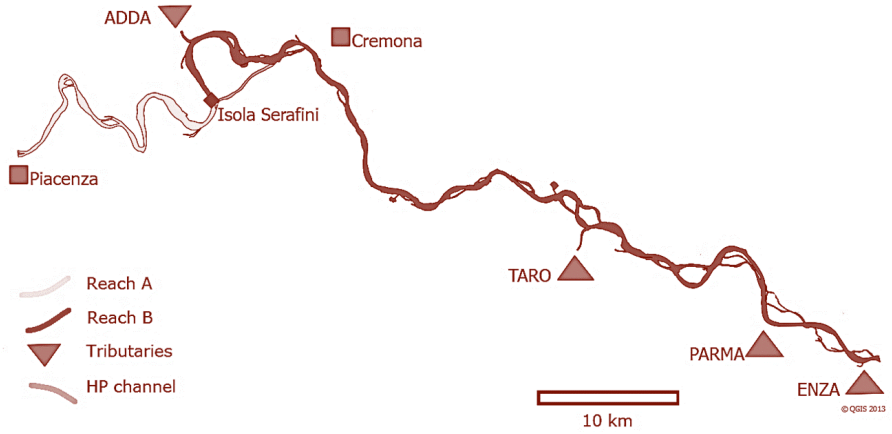

Figure 5.11: Case study area scheme

5.2.1 *Application of the PB model to the case study*

The case study area (Figure 5.11) consists of a 112 km long reach of the Po river: from Piacenza to Boretto.

Cross sections data, available from the 2009 topographical survey by Interregional Po Agency (AIPo), are interpolated over a space interval of 450 m (250 cross sections). A 10 year-long time series of discharges (1964-1973) available from Regional Environmental Agency (ARPA) records has been used both for Po river and the tributary inflows.

The river stretch is then split in two sub-stretches: **A** running for 29 km from Piacenza to IS gate and **B** connecting IS to Boretto 82 km downstream. All 4 tributaries join the river in reach B.

When the HP plant is operating, the two stretches A and B are disconnected. For the upstream stretch A, the downstream boundary condition is the imposed water level; for stretch B the conditions are provided by the gate operation rule: the liquid discharge upstream will be $w = a + u$ while the solid discharge entering the meander, given the solid discharge approaching IS (Q_{sup}), is calculated as follows:

$$Q_{s\,dw} = Q_{s\,up} \cdot 0.7 \cdot \left(\frac{w}{a}\right)^{0.7} \tag{5.6}$$

The reduction coefficient 0.7 takes into account the fact that not all of the eleven gates are open when power station is operating.

On the contrary, when the total discharge a is lower than 300 m^3/s and when it reaches the 4000 m^3/s threshold, the power station stops working, the gate is fully open ($u = 0$) and the two stretches A and B are linked, so that sediment transport continuity is satisfied.

5.3 FRAMEWORK A

The goal of our research is to find a new optimal control law for Isola Serafini. However, even before the optimization procedure can start, a specific framework has to be settled: the shape of the control law, the control mechanism and the decision parameter vector **p** have to be defined.

A first approach is to start maintaining the current control law characteristics and then to apply gradual changes based on the system response. That is what we put into practice in our case study:

We started, in the framework A, from a *feed-forward* control law defined by a parameter vector **p** for a certain class of functions.

Then, having analyzed the system outputs and its response to the new policies, new information on the system behavior became available and a different approach based on a combination of *feed-forward* and *feedback* control appeared to be more effective.

For this reason, at a later stage, a new framework (framework B) was applied to the optimization procedure.

A positive effect on downstream incision could be achieved through two different mechanisms: the increase of the sediment supply to the downstream reach and the increase of the transport capacity in order to lift up the potential settled sediment in the meander.

The former is obtained incrementing the number of dam openings during high flow events, that is by decreasing the threshold value above which the power plant is turned off. The latter can be accomplished by deriving more water to the meander.

In the framework A we design a *feed-forward* control law class of functions able to affect both the sediment supply and the transport capacity.

5.3.1 *The* feed-forward *control law*

We consider the function class of linear piecewise control laws defined by 4 parameters, $\theta_1, \theta_2, \theta_3$ and θ_4 (see Figure 5.12):

$$\begin{cases} u = 0 & \text{if } 0 \leqslant a \leqslant 200 + \text{MEF} \\ u = \min(a - \text{MEF}, 1000) & \text{if } 200 + \text{MEF} < a \leqslant \theta_1 \\ u = \min(\theta_2 + \theta_3 \cdot (a - \theta_1), 1000) & \text{if } \theta_1 < a \leqslant \theta_4 \\ u = 0 & a > \theta_4 \end{cases} \tag{5.7}$$

where u, a and MEF are defined in Section 5.1.3.1.

The parameter θ_4, is the discharge threshold at which the gates are completely open, it primarily affects sediment supply to the down-

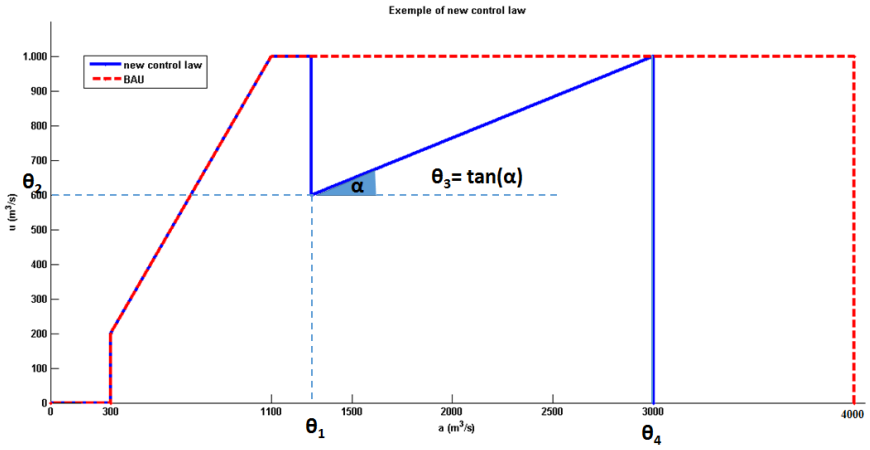

Figure 5.12: Parameters definition

stream reach while θ_1, θ_2 and θ_3 mainly affect the transport capacity in the meander by reducing the discharge u through the turbines.

The current operational rule (also named Business As Usual (BAU)) is associated to a set of instances within this class of functions; precisely to the ones defined by:

$$\begin{cases} \theta_1 \geqslant 300 \\ \theta_2 = 1000 \\ \theta_3 = 0 \\ \theta_4 = 4000 \end{cases} \tag{5.8}$$

The vector $\mathbf{p}$ should be chosen within a certain feasible domain which can be deduced by analyzing the current control law since this already considers the physical constraints: the MEF in the meander, the minimum and maximum flow through the turbines and the safety limit against flood risk. Moreover the function of class considered must take into account the critical flow Q_{crit} below which sediment transport is considered negligible[2].

2 Recent modeling studies on Po river [38] stated this Q_{crit} equals 800 m^3/s. As a caution, we decrease this threshold to 700 m^3/s.

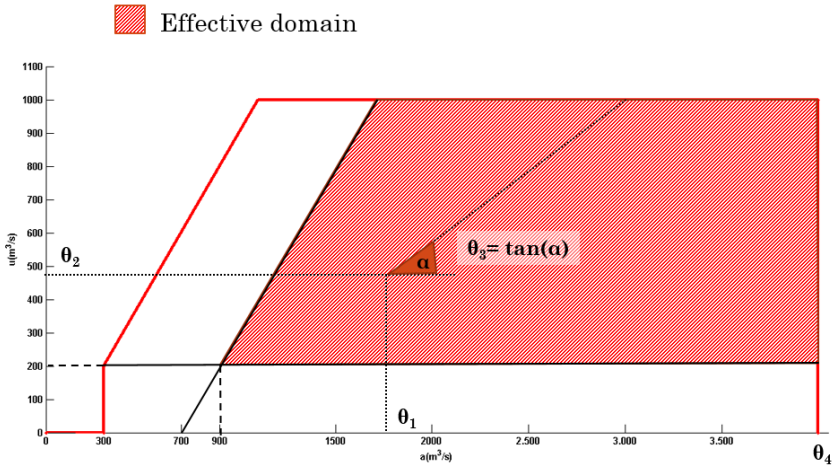

Figure 5.13: The effective domain

The resulting *effective* domain is shown in Figure 5.13 and from it it follows that the feasible set for the parameters θ_1, θ_2, θ_3 and θ_4 is:

$$\begin{cases} 200 \leqslant \theta_4 \leqslant 4000 \\ 900 \leqslant \theta_1 \leqslant \theta_4 \\ 200 \leqslant \theta_2 \leqslant \min(\theta_1 - 700, 1000) \\ 0 \leqslant \theta_3 \leqslant 1 \end{cases} \tag{5.9}$$

5.3.2 *Indicators*

The two conflicting objectives of HP production and riverbed incision are evaluated through suitable indicators.

HYDROPOWER PRODUCTION We consider the revenue J^{HP} which is the product of the daily energy production P_t and the power price α_t at the time t:

$$J_t^{HP} = \alpha_t \cdot P_t \tag{5.10}$$

In turn, the daily production P_t is given by the product of water density ρ, the gravity acceleration g, the flow release u_t through the turbines, the head jump H_t and the turbine efficiency η_t.

$$P_t = \rho g \eta_t u_t H_t \tag{5.11}$$

H_t is the difference between the water level upstream the gate and the level just downstream the turbines ($h_{up} - h_{down}$).

Since the flow profile in the power station channel is not calculated, h_{down} is inferred from an empirical relationship: $h_{down} = f(u, h_{junc})$ where h_{junc} represents the water level at the junction between the channel and the Po river.

INCISION RATE Once the PB model run is over and the final configuration of the bed is known; a low-discharge (300 m^3/s), steady flow simulation is run over both the initial and final bed configurations. The two water surface profiles $z_{final}(\cdot)$ and $z_{initial}(\cdot)$ are then compared to calculate the indicator for riverbed incision. In the considered river stretch connecting Piacenza to Boretto, the area around the city of Cremona is the most significantly affected by bed degradation since its navigation and industrial sectors are suffering big economic damages. Therefore we define the indicator $\mathbf{J}^{INC}$ for the area around Cremona by averaging the water level differences over a 30 cross sections sub-reach:

$$\mathbf{J}^{INC} = \frac{\sum_{l} z_{final}(l) - z_{initial}(l)}{L} \tag{5.12}$$

Where L is the number of cross sections l in the considered sub-reach.

5.3.3 *Optimization*

The MO optimization problem presented in Section 3.1 is solved at each iteration through the RS based approximation described in Chapter 4.

Once discretized the feasible set $\mathcal{P}$, the RS is identified. Since our goal is to contrast riverbed incision without affecting too much the power plant revenue, the Pareto efficient alternatives are identified maximizing both indicators.

5.4 FRAMEWORK B

As it will be shown in Chapter 7, the implementation of framework A produced an insight on the system behavior that induced us to modify the reference framework.

5.4.1 *The* feed-forward *and* feedback *regulator scheme*

In the new framework (framework B) a *feed-forward* and *feedback* regulator scheme (Figure 3.2) is considered.

The *feed-forward* control law is defined over a class of functions in which θ_1, θ_2 and θ_3 have the same value than in the BAU control law, while θ_4 is yearly determined by a *feedback* control law on the base of the observed level of incision.

Therefore the design parameters vector $\mathbf{p}$ is is now composed by the parameters defining the *feedback* control rule. The first three parameters θ_1, θ_2 and θ_3 of the *feed-forward* controller are fixed and the last one (θ_4) is yearly defined by the *feedback* control law.

As explained in Section 3.2, given the difference between the controlled variable and its target value a *feedback* controller manipulates the control in order to reduce this difference in the future. In our case we want to keep a certain yearly incision rate δ. The controlled variable is the observed incision Δ. At the beginning of each year y, on the base of the difference between the observed incision Δ_y and the target incision ($\delta \cdot y$), the controller will determine a new value for the parameter θ_4 of the *feed-forward* control law in the incoming year. More precisely θ_4 in the y^{th} year is given by:

$$\theta_4 = \alpha + \beta \cdot (\Delta_y - \delta \cdot y) \tag{5.13}$$

where α is the value for θ_4 that we presume will produce an yearly incision rate equivalent to δ and β is the gain factor. The design parameters vector is $\mathbf{p} = [\alpha, \beta, \delta]$.

Practically speaking the controller aims to obtain a trajectory for the incision rate Δ_y that follows the line fixed by the target δ (Figure 5.14).

5.4.2 *The indicators*

HYDROPOWER PRODUCTION For HP production, framework B adopts the same indicator of framework A (see Section 5.3.2).

INCISION RATE Since the feedback control rule has to be applied every year, the incision Δ_y must be physically measurable by the DM. The incision rate indicator adopted in the framework A does not satisfy this requirement. That is why we substituted the average difference in water level with the difference Δ_y of the average bed elevation:

$$\Delta_y = H_y - H_0 \tag{5.14}$$

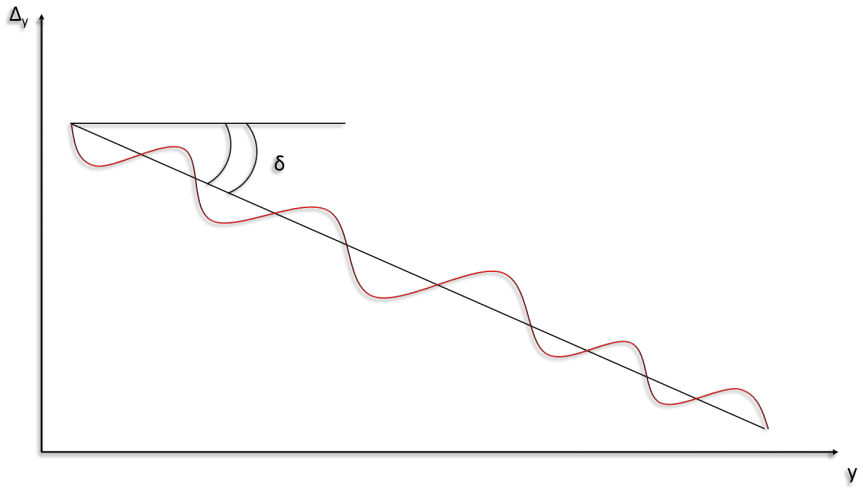

Figure 5.14: The controller effect on the incision rate

where H_t is the average of the five lowest cross section points $b_t^i(l)$ over the 30 sections l considered in the sub-reach around Cremona:

$$H_t = \frac{\sum_{l} \frac{\sum_{i=1}^{5} b_t^i(l)}{5}}{L} \tag{5.15}$$

Being l a single cross section in the considered sub-reach composed by L cross sections.

Consequently, we define the indicator J^{INC} as:

$$J^{INC} = \frac{\sum_{y=0}^{h} \Delta_y}{h} \tag{5.16}$$

where h is the final year in the considered horizon.

5.4.3 *Optimization*

The MO optimization problem is solved through the RS methodology.

Notice that the RS^{INC} is a 4-dimensional surface giving for each vector $\mathbf{p} = [\alpha\, \beta\, \delta]$ the value of the indicator J^{INC}. However given a value of δ, the only alternatives we are interested in are the ones for which the *feedback* control law is effective, in the sense that it produces an incision J^{INC} that is equal to δ. These alternatives are the ones associated to the intersection points between the plane $J^{INC} = \delta$ and the RS^{INC} (see Figure 5.15). Among these points the Pareto-efficient alternative is the one that maximizes the J^{HP} objective.

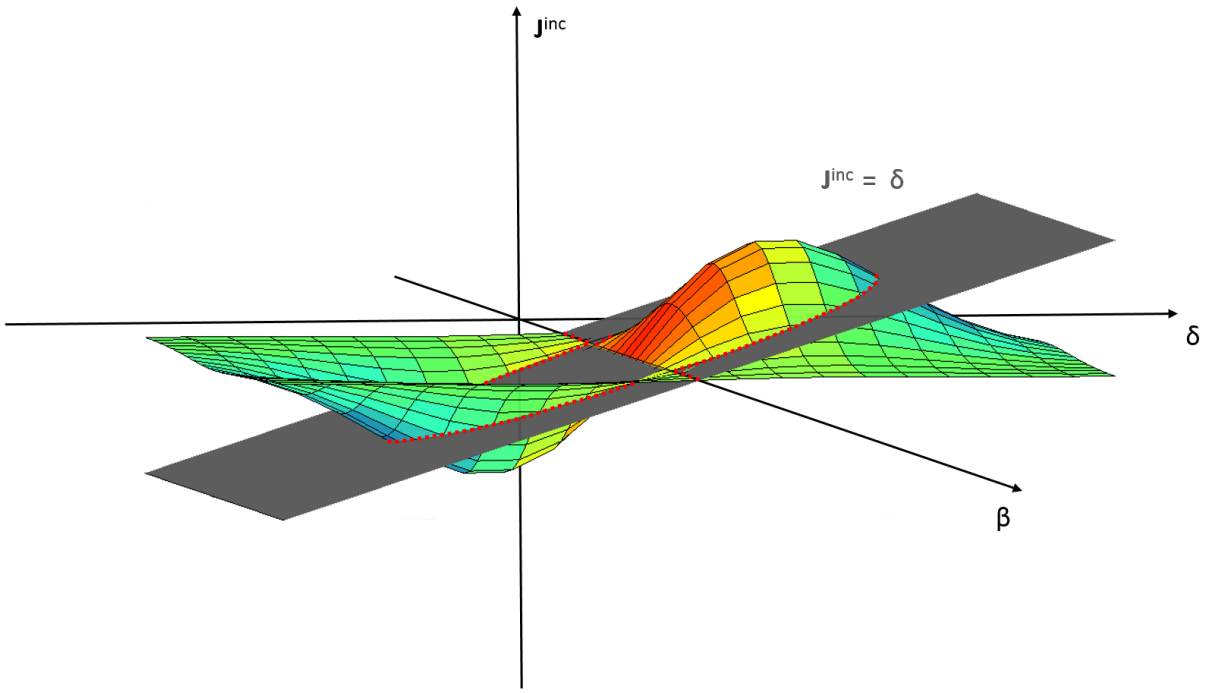

Figure 5.15: Optimization of the incision rate objective based on RS approximation: the optimal solutions (red points) are the intersection points between the plane $\mathbf{I}_h^{INC} = \delta$ and the RS

6

APPLICATION OF THE PROCEDURE TO THE CASE STUDY

6.1 DESIGN OF EXPERIMENT (DOE)

6.1.1 *Framework A*

Before choosing the initial alternative vectors $\mathbf{p} = [\theta_1, \theta_2, \ldots \theta_n]$ to be simulated, the feasible continuous set $\mathcal{P}$ defined by equation 5.9 is discretized.

The feasible set discretisation is operated by means of a hypergrid[1]: each grid point is an element of the discretized set $\mathcal{P}^*$. The hypergrid is made of four equally spaced single grid, one for each parameter θ_i.

In the framework A the cardinality of $\mathcal{P}^*$ is $|\mathcal{P}^*| = 68593$.

The first iteration simulation runs in the framework A are sampled using a heuristic method: we want the sample to be as homogeneous as possible among the feasible set and we also want to investigate the system response to new policies. We select 49 different parameter vectors $\mathbf{p}$ defining as many control laws including the BAU alternative.

6.1.2 *Framework B*

Prior to starting the RS procedure, the *feed-forward* and *feedback* regulator scheme is tested over a small sample of simulations.

This preparatory analysis is useful both for test the regulator scheme effectiveness and to set the feasible domain for the components of the parameter vector $\mathbf{p}$.

In particular:

- α values ranges from 1200 to 4000
- β values ranges from 1000 to 7000
- δ values ranges from -0.06 to 0.06

This feasible continuous set $\mathcal{P}$ is then discretized by a 3-dimensional grid made of 3 homogeneous grids, one for each parameter α, β and δ.

The cardinality of $\mathcal{P}^*$ is $|\mathcal{P}^*| = 22997$.

Afterward, according to our experience on the system behavior, 25 decision vector tuples $\mathbf{p} = [\alpha\ \beta\ \delta]$ are sampled to be simulated at the first iteration.

1 The feasible set has 4 dimensions thus also the hypergrid will be 4-dimensional

6.2 SIMULATION OF THE PB MODEL AND COMPUTATION OF THE INDICATORS

The one-dimensional physical based model presented in Section 5.2 is used to simulate the sampled control laws over a time horizon of 10 years (1964-1973).

In the framework B the controller intervention is set up each year, starting from a BAU configuration for the first year simulation. A yearly intervention is practically applicable and appeared to be effective (as shown in Figure 7.4).

In both frameworks the model outputs are used to evaluate the indicators.

For the present study the simulations were run in parallel on a 8 processors computer; this served a slight reduction of the high computational costs.

6.3 TERMINATION TEST

Starting from the second iteration the termination test can be performed; the test evaluates the distance between the vectors $\widehat{\mathbf{J}}$ of the indicators taken as *interesting* solutions at the previous iteration and the vectors $\mathbf{J}$ of the indicators simulated by the PB model at the current iteration.

If the difference is below a certain threshold λ then the Pareto front based on the RS calculated at the current iteration is considered to be a good approximation of the one that would be generated by the PB model and the procedure is terminated. Else another iteration is performed.

The threshold is chosen accordingly to the type of problem and the adopted indicators; it is about finding the right compromise between the desired accuracy and the available computational power.

In our case the adopted threshold is the 6% of the range of each indicator. This means that we consider correct the values calculated by the RS with a confidence rate of 94%.

6.4 RESPONSE SURFACE IDENTIFICATION

As described in Section 4.1 the Response Surface is a function $\mathbf{f}\ \mathcal{R}^n \rightarrow \mathcal{R}^m$ describing the relation between the n components of the vector $\mathbf{p}$ and the corresponding values of the indicators, i.e. the values of the bi-dimensional vector $\mathbf{J}=\left[J^{HP}\ J^{INC}\right]$.

The term Response Surface can either refers to the vector-valued function RS or to its single scalar components.

In both frameworks we considered two indicators (J^{HP}, J^{INC}) which means two different scalar RS approximations (RS^{HP}, RS^{INC}) have to be identified at each iteration.

Identifying the RS is nothing other than a traditional model identification problem, as such it is composed of model selection (the function class of the RS), calibration (estimation of the parameters, when present) and model validation, reiterated at each iteration over the updated data set.

For the present study the model identification is performed using the cross-validation technique[2].

The data set available from the model simulations at the k-th iteration is first normalized by scaling between 0 and 1 and then randomly partitioned into a training set and a validation set. For each class of functions considered a RS is identified and a validation error is computed. The random partitioning is reiterated for a certain amount of times and the validation results are averaged over the rounds. The function class with the lowest average error in validation is then chosen.

We considered two different function classes: linear interpolation and Radial Basis Function (RBF) combined with different parameters. In total five different types of function were tested for each indicator at each iteration:

- linear interpolation
- RBF of the forms
  - Gaussian
  - Thin plate spline
  - Multiquadratic
  - Cubic

In the following sections the aforementioned function classes will be described in detail.

2 Cross-validation is a model validation technique for assessing how the results of a statistical analysis will generalize to an independent data set. One round of cross-validation involves partitioning a sample of data into complementary subsets, performing the analysis on one subset (called the training set), and validating the analysis on the other subset (called the validation set or testing set). To reduce variability, multiple rounds of cross-validation are performed using different partitions, and the validation results are averaged over the rounds.

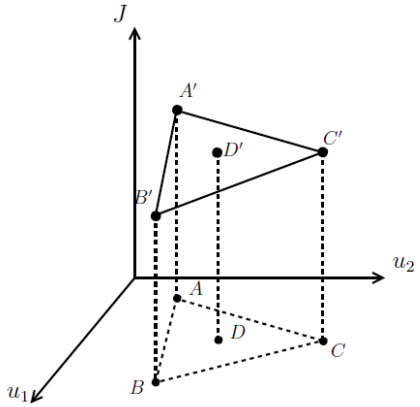

Figure 6.1: Delaunay triangulation method

6.4.1 *Linear interpolation*

The linear n-dimensional interpolation over a non-uniformly-spaced grid is based on the Delaunay[3] triangulation method.

To introduce Delaunay triangulation method we start presenting the 2-dimensional case. The same procedure can be easily extended to the n-dimensional case.

In the 2-dimensional case the RS would define the relation between the indicator J and the vector $\mathbf{p} = [p_1, p_2]$; Delaunay triangulation defines a triangular net in the (p_1, p_2) space such as no point of the grid is inside the circumcircle of any triangle. Moreover the minimum angle of all the angles of the triangles is maximized.

Using the values of J given by the simulation runs (training set) the triangle can be mapped in the 3-dimensional space (p_1, p_2, J). The interpolation method is described in Figure 6.1: we consider the triangle having vertex A, B, C in the parameter space; the corresponding indicator values are known and mapped in A', B', C' and the plane function $J = f_{ABC}(p_1, p_2)$ can be inferred. Using this function we can calculate the indicator value for each point inside the triangle. For example D is mapped into D' where $J_D = f_{ABC}(p_1^D, p_2^D)$.

In our multidimensional case, Delaunay triangulation defines a n-dimensional hyper-triangular net in the parameter space; the interpolated indicator value is given by the hyper-plane function of the considered hyper-triangle.

One limitation of this method is that it cannot extrapolate, that is to calculate J values outside the given triangular grid.

3 Boris Nikolaevich Delaunay (1890 – 1980) was a Soviet/Russian mathematician involved in the fields modern algebra and geometry of numbers. He invented what is now called Delaunay triangulation in 1934.

We overcome this problem replacing each missing value with the closest one (euclidean distance).

6.4.2 *Radial basis functions*

RBF models consist of a weighted simple summation of radial basis functions and a polynomial.

The RB functions are first trained with the available simulated data pairs ($\mathbf{p}$, J) in order to reproduce the current correlation between decision parameters and the system response.

The model is then composed of n RBF where n is the number of given data pairs ($\mathbf{p}$, J). When an input $\mathbf{p}$ is given to the model, each function generates a weight which is summed and processed to produce the output.

The different forms of RBF are all based on a scalar radius. In our case it is the Euclidean norm $\|\cdot\|$ of the input data $\mathbf{p}$ and the center nodes $\mathbf{c}$, where each center node $\mathbf{c}$ corresponds to one data pair ($\mathbf{p}$, J) from the training set.

Many different RBF are available, in particular we tested:

- Gaussian

$$\varphi = \exp\left(-\frac{\|\mathbf{p}-\mathbf{c}\|^2}{\sigma^2}\right) \tag{6.1}$$

- multiquadratic

$$\varphi = \sqrt{1+\frac{\|\mathbf{p}-\mathbf{c}\|^2}{2\sigma^2}} \tag{6.2}$$

- cubic

$$\varphi = \|\mathbf{p}-\mathbf{c}\|^3 \tag{6.3}$$

- thin plate spline

$$\varphi = \|\mathbf{p}-\mathbf{c}\|^2 \ln\left(\|\mathbf{p}-\mathbf{c}\|+1\right) \tag{6.4}$$

RBF models can be seen as a simple Artiicial Neural Networks (ANN) composed of only three layers: an *input* layer which feeds the *hidden* layer (adopting RBF as activation functions) and an *output* layer processing the produced weights.

RBF models are fast performing and can achieve a satisfactory approximation on the basis of a small training set.

6.5 MO OPTIMIZATION

A different optimization procedure is adopted in the two frameworks as described in detail in Sections 5.3.3 and 5.4.3.

6.6 SELECTION OF *interesting* ALTERNATIVES

As mentioned in Section 4.3.5 the selection of *interesting* alternatives can be performed by an expert or by means of automatic selection techniques.

In our case the former method has been adopted: the selection was based on our experience on the system behavior and the optimization techniques.

7 RESULTS

This chapter presents the results obtained by applying the procedure proposed in Chapter 4 to the case study described in Chapter 5 following the techniques presented in Chapter 6 at each procedural step.

All the analysis were implemented by means of the MATLAB computing software [24].

7.1 FRAMEWORK A

7.1.1 *Initialization*

The feasible domain $\mathcal{P}^*$ is sampled using a heuristic method: since θ_4 represents the flow threshold above which the gates are fully open, experiments with different values for this parameter are useful to assess the importance of restoring sediment connectivity between upstream and downstream more frequently.

At the same way, implementing different values of θ_1,θ_2 and θ_3 can show the effects of increasing transport capacity in the meander.

We chose to simulate 49 different instances of vector $\mathbf{p}$ including the BAU alternative.

Each parameter vector $\mathbf{p} = [\theta_1, \theta_2, \ldots \theta_n]$ defines a specific control law. Figure 7.1 shows the first set of simulated control laws.

This may appear a high number of initial model runs, however, in this first phase, these simulations are useful also to understand the

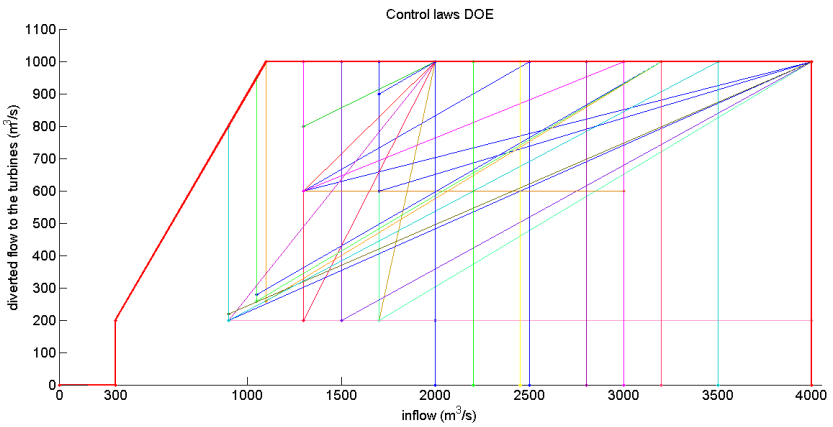

Figure 7.1: DOE: 49 different well distributed control laws are chosen among the feasible discretized set $\mathcal{P}^*$

system behavior: it is the first time that the model is used to simulate the Po river and the IS system.

7.1.2 *First iteration*

The first iteration, unlike the others, does not perform a termination test.

7.1.2.1 *Simulation runs*

The 49 initial alternatives are simulated by means of the physical based model.

The model outputs are elaborated to produce the indicator values J^{HP} and J^{INC}.

The Table 7.1 shows the results.

7.1.2.2 *Response surface identification*

The simulated indicator values $\mathbf{J}$ are used to identify the best RS interpolation for each indicator using the cross-validation algorithm presented in Section 6.4.

The cross-validation results for each indicator and each function type is presented in Table 7.2. Note that the indicator values are first normalized by scaling between 0 and 1.

The best performance is given by the cubic RBF model for J^{HP} and by the multiquadratic RBF model for J^{INC}.

Therefore these two interpolations are adopted to generate RS^{HP} and RS^{INC} respectively using the non-normalized simulation as training set and the discretized feasible domain $\mathcal{P}^*$ as input. The outcome is a series of 68593 approximated $\hat{\mathbf{J}}$ values, one for each $\mathbf{p}$ combination in the $\mathcal{P}^*$ set.

7.1.2.3 *Pareto front*

The Pareto-efficient alternatives are then identified according to their approximated performance $\hat{\mathbf{J}}$.

Over 68593 alternatives 341 are Pareto dominant. Figure 7.2 shows these alternatives composing the Pareto front.

Note that both indicators have to be maximized.

7.1.2.4 *Selection of interesting points*

Interesting alternatives are chosen among the Pareto-efficient ones considering both their physical meaning (the related control laws) and their proximity to the Pareto front *knee*.

We selected 8 *interesting* alternatives to be simulated at the next iteration.

θ_1	θ_2	θ_3	θ_4	J^{HP} (10^6€/y)	J^{INC} (m/10y)
1700	1000	0	4000	34.2805	-0.5179
1700	200	0	2000	31.5653	0.0897
1700	200	100	2000	31.6258	0.086
1700	200	0	4000	31.94	-0.4942
1700	200	100	4000	33.1793	-0.5522
1700	1000	0	2000	32.2661	0.0641
1700	1000	0	3000	33.9733	-0.3049
1700	600	100	4000	33.9659	-0.5211
900	200	50	2000	25.1594	0.1199
1300	600	100	4000	33.5202	-0.5482
1300	600	100	2000	31.5279	0.0656
900	200	0	4000	23.3899	-0.5897
1500	200	100	4000	32.5701	-0.5478
900	200	25	4000	25.3195	-0.6792
900	200	75	4000	28.2102	-0.6302
900	200	100	2500	28.3264	-0.1757
900	200	100	3500	29.0291	-0.5392
1300	600	50	3000	32.8009	-0.3127
900	200	0	3000	23.3275	-0.3917
1300	600	100	2200	32.084	-0.0404
1300	600	100	2500	32.7175	-0.1287
1300	600	100	3000	33.2132	-0.3245
1300	800	100	2000	32.0741	0.0593
1300	400	100	2000	30.7096	0.1019

θ_1	θ_2	θ_3	θ_4	J^{HP} (10^6€/y)	J^{INC} (m/10y)
1000	260	100	2500	29.5096	-0.1678
1050	260	100	3200	30.4284	-0.4414
1300	600	0	3000	31.6472	-0.2471
1300	600	25	3000	32.3628	-0.3245
1300	600	75	3000	33.0495	-0.3184
1100	260	100	3200	30.7947	-0.424
1050	280	100	3200	30.5996	-0.4425
1050	260	90	3200	30.2045	-0.4414
1050	260	100	3700	30.5951	-0.5769
900	200	100	2000	27.1164	0.0553
1200	320	100	2000	29.9232	0.1074
1200	320	100	3000	31.5996	-0.3202
1200	1000	0	2000	32.2661	0.0641
1200	1000	0	3000	33.9733	-0.3049
1250	320	100	3000	31.8278	-0.3117
1200	340	100	3000	31.7203	-0.3202
1200	320	90	3000	31.4552	-0.3225
1200	320	100	3500	31.7991	-0.313
900	200	100	4000	29.1369	-0.6092
950	200	100	4000	29.4218	-0.6193
1000	200	100	4000	29.7343	-0.6224
900	220	100	4000	29.376	-0.6028
900	200	90	4000	28.7969	-0.6175
900	200	100	3500	29.0291	-0.5392

Table 7.1: 1^{st} iteration simulation runs (framework A)

Interpolator	J^{HP}	J^{INC}
Linear interpolator	0.0025	0.0032
RBF Gaussian	0.0032	26.3953
RBF Thin plate	0.0010	0.0043
RBF Cubic	**0.0009**	0.0344
RBF Multiquadratic	0.0011	**0.0030**

Table 7.2: Cross validation results: mean errors for the 5 interpolation functions tested for the 1^{st} iteration (framework A)

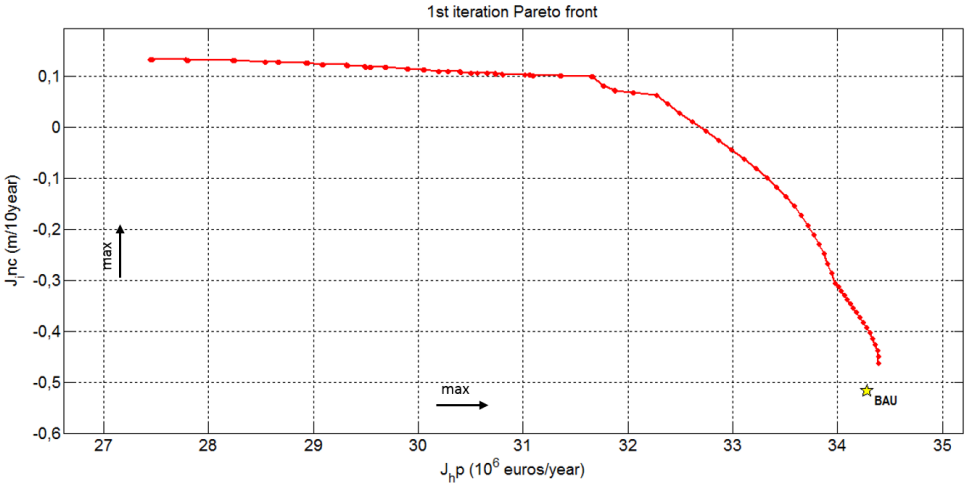

Figure 7.2: 1^{st} iteration Pareto front: the Pareto front (red line) and the Pareto-efficient alternatives (red dots) obtained by means of RS approximation are compared with the BAU alternative (star)

θ_1	θ_2	θ_3	θ_4	$\hat{J}^{HP}$ (10^6€/y)	$\hat{J}^{INC}$ (m/10y)
1700	1000	0	3200	34.0875	-0.3365
1700	1000	0	2800	33.8187	-0.2289
1700	1000	0	2450	33.3215	-0.0983
1700	1000	0	2200	32.7393	-0.0070
1700	1000	0	2000	32.2661	0.0641
1700	900	1	2000	31.8736	0.0726
1700	400	0.3	2000	31.6462	0.1004
1400	400	0.5	2000	29.6865	0.1178

Table 7.3: Selected alternatives for the 2^{nd} iteration (framework A)

Table 7.3 shows the selected alternatives together with the respective $\hat{\mathbf{J}}$ values.

7.1.3 *Second iteration*

7.1.3.1 *Simulation runs*

The 8 alternatives chosen at the previous iteration are simulated by means of the PB model.

The model outputs are used to calculate the indicator values shown in Table 7.4.

7.1.3.2 *Termination test*

From the second iteration on we can perform the termination test.

θ_1	θ_2	θ_3	θ_4	J^{HP} (10^6€/y)	J^{INC} (m/10y)
1700	1000	0	3200	34.0669	-0.3599
1700	1000	0	2800	33.8321	-0.2311
1700	1000	0	2450	33.3977	-0.0855
1700	1000	0	2200	32.8347	-0.0408
1700	1000	0	2000	32.2661	0.0641
1700	900	1	2000	32.2520	0.0646
1700	400	0.3	2000	31.7793	0.0917
1400	400	0.5	2000	31.7916	0.0916

Table 7.4: 2^{nd} iteration model outcomes (framework A)

As described in Section 6.3 the 8 *interesting* alternatives identified by RS approximation in the first iteration are compared to the ones calculated by means of the PB model.

The average of the 8 calculated absolute differences $\left|J - \hat{J}\right|$ has to be evaluated for both indicators with respect to the threshold λ which is the 6% of the range of each indicator.

As shown in Table 7.5 both average absolute differences are below the given thresholds.

This means that the wanted approximation confidence rate has been accomplished and we can terminate the RS approximation procedure at the second iteration.

7.1.3.3 *Response surface identification*

The 8 new simulated alternatives join the previous 49 data pairs and the procedure for the identification of the best RS interpolation is repeated.

The cross-validation results for each indicator and each function type is presented in Table 7.6.

Once again the best performance is given by the cubic RBF model for J^{HP} and by the multiquadratic RBF model for J^{INC}.

These two interpolations are then adopted to generate RS^{HP} and RS^{INC} respectively using the 57 simulation as training set and the discretized feasible domain $\mathcal{P}^*$ as input.

7.1.3.4 *Pareto front*

Over 68593 alternatives 111 are identified as Pareto-efficient. Figure 7.3 shows these alternatives composing the Pareto front.

	θ_1	θ_2	θ_3	θ_4	ΔJ^{HP} (10^6€/y)	ΔJ^{INC} (m/10y)
	1700	1000	0	3200	0.0205	0.0234
	1700	1000	0	2800	0.0134	0.0022
	1700	1000	0	2450	0.0762	0.0128
	1700	1000	0	2200	0.0954	0.0337
	1700	1000	0	2000	0.0000	0.0000
	1700	900	1	2000	0.3784	0.0080
	1700	400	0.3	2000	0.1331	0.0087
	1400	400	0.5	2000	2.1051	0.0262
|**average**|					**0.3528**	**0.0144**

J	RANGE	λ (6% threshold)
$\hat{J}_{hp}(10^6€/y)$	11.1245	**0.66747**
$\hat{J}_{inc}(m/10y)$	0.903	**0.05418**

Table 7.5: 2^{nd} iteration termination test (framework A)

Interpolator	J^{HP}	J^{INC}
Linear interpolator	0.0017	0.0031
RBF Gaussian	0.0064	12.0689
RBF Thin plate	0.0009	0.0096
RBF Cubic	**0.0007**	0.0098
RBF Multiquadratic	0.0120	**0.0025**

Table 7.6: Cross validation results: mean errors for the 5 interpolation functions tested for the 2^{nd} iteration (framework A)

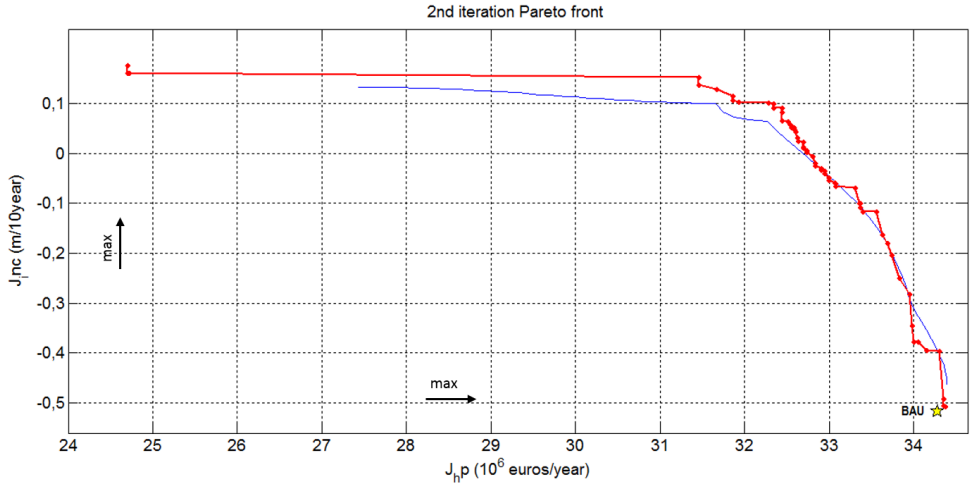

Figure 7.3: 2^{nd} iteration Pareto front: the Pareto front (red line) and the Pareto-efficient alternatives (red dots) obtained by means of RS approximation are compared with the Pareto front from the previous iteration (blue line) and the BAU alternative (star)

7.1.4 *Results analysis*

Both Figures 7.2 and 7.3 show the simulated BAU alternative performance (star): the current control law leads to a yearly hydropower generation revenue of $34.2810^6€/year$ and to an incision rate J^{INC} in Cremona of -0.52 m in ten years.

The trade offs inferred from both Pareto fronts show that there are several possibilities for considerably reducing the incision process in Cremona with a moderate loss in hydroelectricity production.

The rapid convergence of the Pareto front shown in Figure 7.3 is due to the numerous elements of the initial training set.

As already mentioned many simulations were necessary to initially test the model performance for the case study and to understand the system behavior.

In this perspective both simulated and approximated results had revealed a characteristic system response: θ_4 turned out to be the most sensitive driver of river bed evolution.

The best performing alternatives (the ones with the best J^{HP}/J^{INC} trade off) where the ones operating the current control law 5.8 with a different high flow threshold θ_4. On the contrary, changes in θ_1, θ_2 and θ_3 led up to substantial reduction in hydropower production without relevantly affecting river incision.

From these results a certain hypothesis on the existing correlation between the decision variables $\mathbf{p}$ and the indicator J^{INC} can be inferred: it's possible that only high flow events and the restored sedi-

variable	γ	p-value
$\theta 1$	$9.51 \cdot 10^{-}5$	$9.92 \cdot 10^{-}5$
$\theta 4$	$-3.22 \cdot 10^{-}4$	$4.09 \cdot 10^{-}40$

Table 7.7: Regression analysis: γ coefficients and p-values

ment flow connection can effectively influence the incision rate downstream.

To verify this hypothesis a regression analysis is performed over the simulated data.

7.1.4.1 *Regression analysis of simulated data*

A stepwise linear regression is performed over the simulated data (57 simulations) in order to infer the correlation between the decision parameters θ_n and the incision rate J^{INC}.

The results are shown herein:

step 0 no predictor included. Adjusted $R^2 = 0$

step 1 θ_4 is added as input. Adjusted $R^2 = 0.955168$

step 2 θ_1 is added as input. Adjusted $R^2 = 0.96543$

Final linear regression model:

$$J^{INC} = 1 + \gamma_1 \theta_1 + \gamma_4 \theta_4 \tag{7.1}$$

where $\gamma_{1,\dots,4}$ are the estimated coefficients shown in Table 7.7 together with the respective p-value[1]:

7.1.5 *Conclusions*

The stepwise regression analysis showed that only the θ_4 / J^{INC} correlation is significant.

From both Pareto front and regression analysis it can be inferred that acting only on sediment transport capacity in the meander is ineffective in stopping incision and, at the same time, it conflicts with electricity production.

1 Most regression methods perform a statistical test for the coefficients associated with each independent variable. The null hypothesis for this statistical test states that a coefficient is not significantly different from zero (in other words, for all intents and purposes, the coefficient is zero and the associated explanatory variable is not helping your model). Small p-values reflect small probabilities, and suggest that the coefficient is, indeed, important to your model with a value that is significantly different from zero

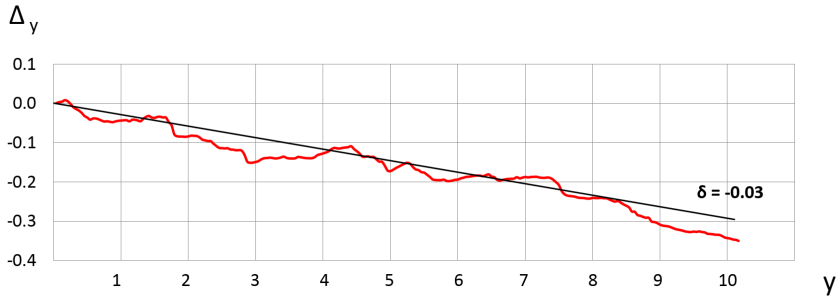

Figure 7.4: Framework B control scheme performance: the yearly incision rate Δ_y trend (in red) is kept close to the target line (in black). In this example $\alpha = 3700$, $\beta = 4000$ and $\delta = -0.03$

On the contrary, increasing sediment supply employing high flow events appeared to be very effective in contrasting riverbed incision: high flow events are usually rare and short-lived, however they bring a lot of sediment from upstream. A decreased high flow threshold θ_4 would increase the number of short gates openings thus promoting sediment flow connection without affecting too much the HP production.

Therefore new framework based on θ_4 control could lead to better trade offs.

7.2 FRAMEWORK B

Prior to applying the RS procedure, we run some simulations in order to test the performance of the *feed-forward* and *feedback* regulator scheme. If the scheme will turn out to be effective, these simulation runs will be used as part of the initial training set.

As shown in Figure 7.4 the double control law regulator behaves as expected, keeping the yearly incision rate Δ_y trend close to the target line.

7.2.1 *Initialization*

The alternatives to be simulated at the first iteration are sampled homogeneously among the discrete feasible set $\mathcal{P}^*$ defined in Section 6.1.2.

Over 22997 feasible parameter combinations 25 alternatives are selected.

α	β	δ	J^{HP} (10^6€/y)	J^{INC} (m/10y)
1900	2500	-0.01	32.60834	0.01
1900	5500	-0.01	33.28765	0.00
2700	5500	-0.01	33.29510	-0.02
1900	5500	-0.03	32.79383	-0.01
2700	2500	-0.03	33.56657	-0.02
3500	5500	-0.03	33.58043	-0.03
2700	2500	-0.05	33.61492	-0.03
2700	5500	-0.05	33.50666	-0.02
3500	2500	-0.05	34.02171	-0.04
2700	2500	-0.01	33.53650	-0.02
2700	5500	-0.03	33.37644	-0.02
3500	2500	-0.03	34.01162	-0.04
3500	5500	-0.05	33.60820	-0.03
2300	4000	0	33.45887	-0.01
2300	4000	-0.01	33.30094	-0.01
2300	4000	-0.03	33.18360	-0.01
3100	4000	-0.01	33.64319	-0.03
3100	4000	-0.03	33.65685	-0.03
3100	4000	-0.05	33.77410	-0.03
3100	4000	-0.04	33.71416	-0.03
2700	3000	0	33.49993	-0.02
3700	4000	-0.03	34.04090	-0.03
3500	5000	-0.01	33.72562	-0.03
2300	5000	0.01	33.4432	0
1900	2500	-0.03	32.92350	0.01

Table 7.8: 1st iteration model outcomes (framework B)

7.2.2 *First iteration*

7.2.2.1 *Simulation runs*

The 25 initial alternatives are simulated by means of the physical based model.

The model outputs are elaborated to produce the indicator values J^{HP} and J^{INC}.

The Table 7.8 shows the results.

7.2.2.2 *Response surface identification*

The simulated indicator values **J** are used to identify the best RS interpolation for each indicator using the cross-validation algorithm presented in Section 6.4.

Interpolator	J^{HP}	J^{INC}
Linear interpolator	$6.57 \cdot 10^{-}5$	0.027939594
RBF Gaussian	48402.86697	0.017392447
RBF Thin plate	0.004897438	0.014390739
RBF Cubic	1174.825286	0.01529649
RBF Multiquadratic	$\mathbf{4.76 \cdot 10^{-5}}$	**0.014187965**

Table 7.9: Cross validation results: mean errors for the 5 interpolation functions tested for the 1^{st} iteration (framework B)

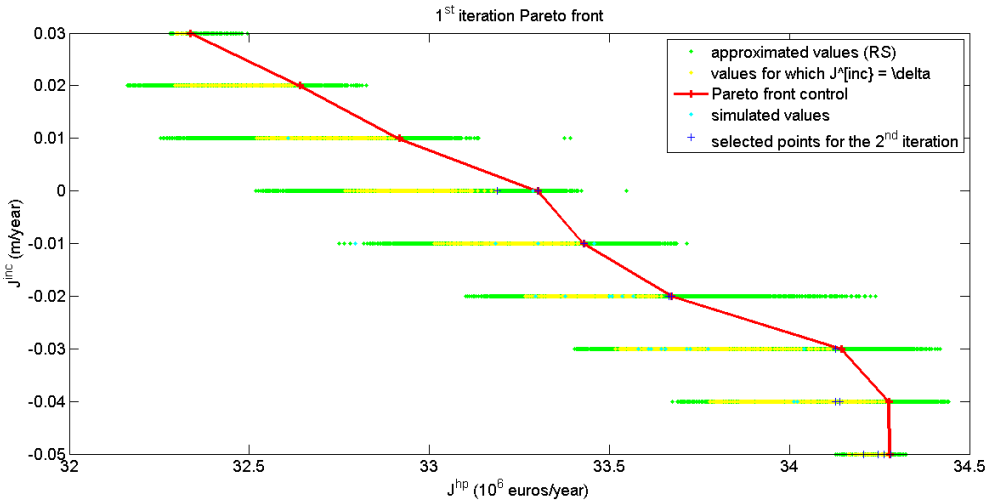

Figure 7.5: 1^{st} iteration Pareto front (red line): the 22997 $\hat{J}^{INC}$ values generated by the RS approximation are rounded to two decimal places (green points), among these alternatives we identify the ones having $\hat{J}^{INC} = \delta$ (yellow points). The Pareto efficient alternatives are the ones maximizing $\hat{J}^{HP}$ (red points)

The cross-validation results for each indicator and each function type is presented in Table 7.9. Note that the indicator values are first normalized by scaling between 0 and 1.

The RBF Multiquadratic interpolation turned out to be the best performing for both the indicators and was used to identify the two approximated RS.

7.2.2.3 *Pareto front*

Over the 22997 feasible alternatives generated by the RS approximation only the ones having $\hat{J}^{INC} = \delta$ are selected. Note that $\hat{J}^{INC}$ values are first rounded to two decimal places.

Among these alternatives the Pareto efficient are the ones maximizing $\hat{J}^{HP}$. The pareto front obtained from the 1^{st} iteration is shown in Figure 7.5.

α	β	δ	$\hat{J}^{HP}$ (10^6€/y)	$\hat{J}^{INC}$ (m/10y)
4000	1000	-0.06	34.20510964	-0.05
2100	4200	0	33.18921859	0
3900	4100	-0.03	34.12751628	-0.03
3900	4000	-0.04	34.12925165	-0.04
3100	1000	-0.02	33.66640928	-0.02
3100	1100	-0.02	33.67266722	-0.02
2500	4000	-0.01	33.42827078	-0.01
1900	5500	0	33.30242448	0
4000	1500	-0.05	34.24640715	-0.05
3900	3800	-0.05	34.14043531	-0.04
4000	2200	-0.06	34.26160511	-0.05

Table 7.10: Selected alternatives for the 2^{nd} iteration (framework B)

α	β	δ	J^{HP} (10^6€/y)	J^{INC} (m/10y)
4000	1000	-0.06	34.24873	-0.06
2100	4200	0	32.98339	0.00
3900	4100	-0.03	33.94099	-0.04
3900	4000	-0.04	33.99602	-0.05
3100	1000	-0.02	33.96922	-0.04
3100	1100	-0.02	33.96392	-0.04
2500	4000	-0.01	33.26575	-0.02
1900	5500	0	33.19322	0.00
4000	1500	-0.05	34.23303	-0.06
3900	3800	-0.05	34.03750	-0.04
4000	2200	-0.06	34.21082	-0.06

Table 7.11: 2^{nd} iteration model outcomes (framework B)

7.2.2.4 *Selection of interesting points*

We select 11 new alternatives to be simulated at the next iteration (blue crosses in Figure 7.5). The alternatives together with their approximated performances are displayed in Table 7.10.

7.2.3 *Second iteration*

7.2.3.1 *Simulation runs*

The 11 alternatives chosen at the previous iteration are simulated by means of the PB model.

The model outputs are used to calculate the indicator values shown in Table 7.11.

	α	β	δ	ΔJ^{HP} (10^6€/y)	ΔJ^{INC} (m/10y)
	4000	1000	-0.06	-0.043618361	0.013793548
	2100	4200	0	0.205829587	-0.000922581
	3900	4100	-0.03	0.186528277	0.013374194
	3900	4000	-0.04	0.133234653	0.00503871
	3100	1000	-0.02	-0.302814719	0.019187097
	3100	1100	-0.02	-0.291254783	0.016993548
	2500	4000	-0.01	0.162525776	0.006258065
	1900	5500	0	0.109202479	0.001451613
	4000	1500	-0.05	0.013374153	0.011509677
	3900	3800	-0.05	0.102931315	0.004935484
	4000	2200	-0.06	0.050790107	0.007251613
|average|				**0.02970**	**0.00899**

J	RANGE	λ (6% threshold)
$\hat{J}_{hp}$(10^6€/y)	1.8763	**0.112578**
$\hat{J}_{inc}$(m/10y)	0.09	**0.0054**

Table 7.12: 2^{nd} iteration termination test (framework B)

7.2.3.2 *Termination test*

A termination test is then performed: the 11 *interesting* alternatives identified by RS approximation in the first iteration are compared to the simulated ones; the results are shown in Table 7.12 .

The average of the 11 calculated absolute differences $\left|J - \hat{J}\right|$ has to be evaluated for both indicators with respect to the threshold λ which is the 6% of the range of each indicator.

Since the average absolute difference for $\hat{J}^{INC}$ is below its threshold the RS approximation procedure has to be reiterated.

7.2.3.3 *Response surface identification*

The best response surface interpolation for the 2^{nd} iteration is then identified. The results from the cross-validation procedure presented in Table 7.13 show that the best performing interpolation for both indicators is once again a RBF Multiquadratic model.

7.2.3.4 *Pareto front*

Similarly to the previous iteration the Pareto front is identified as shown in Figure 7.6.

Interpolator	J^{HP}	J^{INC}
Linear interpolator	$4.14 \cdot 10^{-}5$	0.016957488
RBF Gaussian	776031.7272	15982482.42
RBF Thin plate	0.007399197	0.772768366
RBF Cubic	116.7465058	7265.747692
RBF Multiquadratic	$\mathbf{2.54 \cdot 10^{-5}}$	**0.006379166**

Table 7.13: Cross validation results: mean errors for the 5 interpolation functions tested for the 2^{nd} iteration (framework B)

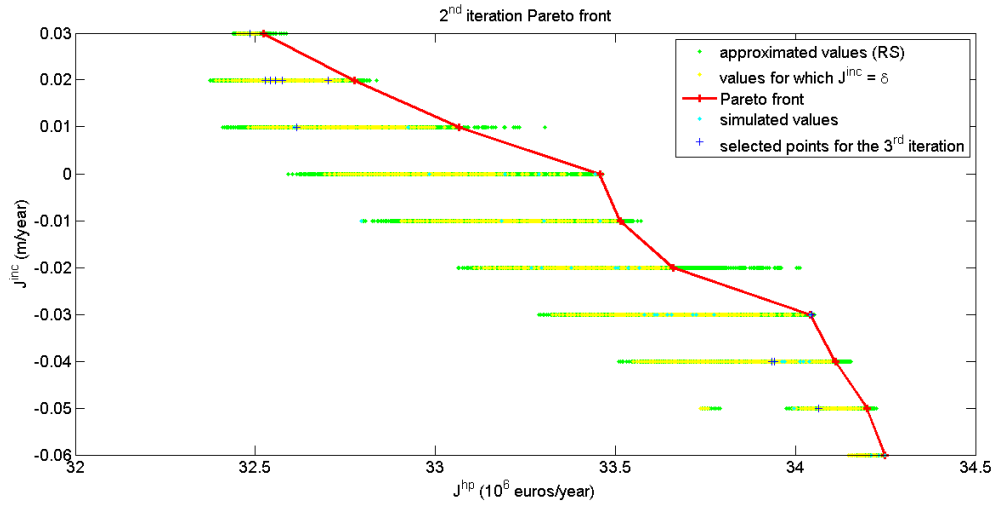

Figure 7.6: 2^{nd} iteration Pareto front (red line): the 22997 $\hat{J}^{INC}$ values generated by the RS approximation are rounded to two decimal places (green points), among these alternatives we identify the ones having $\hat{J}^{INC} = \delta$ (yellow points). The Pareto efficient alternatives are the ones maximizing $\hat{J}^{HP}$ (red points)

α	β	δ	$\hat{J}^{HP}$ (10^6€/y)	$\hat{J}^{INC}$ (m/10y)
1300	3600	0.01	32.55560658	0.02
1200	3500	0.03	32.48628858	0.03
1400	6000	0.02	32.61565294	0.01
1300	2000	0.02	32.57587845	0.02
1200	1000	0.04	32.70318756	0.02
3300	2000	-0.04	33.93381018	-0.04
3900	4500	-0.05	33.94191933	-0.04
4000	3800	-0.05	34.06428318	-0.05
1200	2000	0.02	32.52656183	0.02
1300	3500	0.03	32.54132522	0.02

Table 7.14: Selected alternatives for the 3rd iteration (framework B)

α	β	δ	J^{HP} (10^6€/y)	J^{INC} (m/10y)
1300	3600	0.01	32.50947	0.03
1200	3500	0.03	32.36372	0.03
1400	6000	0.02	32.68517	0.02
1300	2000	0.02	32.02588	0.05
1200	1000	0.04	30.86234	0.06
3300	2000	-0.04	33.99422	-0.03
3900	4500	-0.05	33.89117	-0.05
4000	3800	-0.05	34.07695	-0.05
1200	2000	0.02	31.83003	0.05
1300	3500	0.03	32.40405	0.03

Table 7.15: 3rd iteration model outcomes (framework B)

7.2.3.5 *Selection of interesting points*

Ten interesting alternatives are selected to be simulated at the next iteration (Table 7.14).

7.2.4 *Third iteration*

7.2.4.1 *Simulation runs*

The 10 interasting alternatives selected at the previous iteration are simulated. The results are shown in Table 7.15.

7.2.4.2 *Termination test*

The termination test is then performed (Table 7.16): since both the average absolute differences turned out to be above the respective threshold the RS approximation procedure has to be reiterated.

	α	β	δ	ΔJ^{HP} (10^6€/y)	ΔJ^{INC} (m/10y)
	1300	3600	0.01	0.046138579	-0.011341935
	1200	3500	0.03	0.122573576	-0.004580645
	1400	6000	0.02	-0.069520056	-0.007070968
	1300	2000	0.02	0.549999448	-0.025367742
	1200	1000	0.04	1.840846561	-0.044980645
	3300	2000	-0.04	-0.060408824	-0.005922581
	3900	4500	-0.05	0.050750331	0.00776129
	4000	3800	-0.05	-0.012664825	-0.000541935
	1200	2000	0.02	0.696527834	-0.025445161
	1300	3500	0.03	0.137277219	-0.013948387
|average|				**0.33015**	**0.01314**

J	RANGE	λ (6% threshold)
$\hat{J}_{hp}$(10^6€/y)	3.4226	**0.239582**
$\hat{J}_{inc}$(m/10y)	0.12	**0.0072**

Table 7.16: 3rd iteration termination test (framework B)

Interpolator	J^{HP}	J^{INC}
Linear interpolator	0.000116634	0.0072825
RBF Gaussian	33440.07113	22376563.87
RBF Thin plate	0.001512785	2.153911217
RBF Cubic	62.76935622	2306899.419
RBF Multiquadratic	**$7.97 \cdot 10^{-5}$**	**0.003067986**

Table 7.17: Cross validation results: mean errors for the 5 interpolation functions tested for the 3rd iteration (framework B)

7.2.4.3 *Response surface identification*

Once again a RBF Multiquadratic model is selected as the best performing interpolation for both indicators (Table 7.17).

7.2.4.4 *Pareto front*

A new Pareto front (Figure 7.7) is identified.

7.2.4.5 *Selection of interesting points*

We select 12 interesting alternatives to be simulated at the next iteration (Table 7.18).

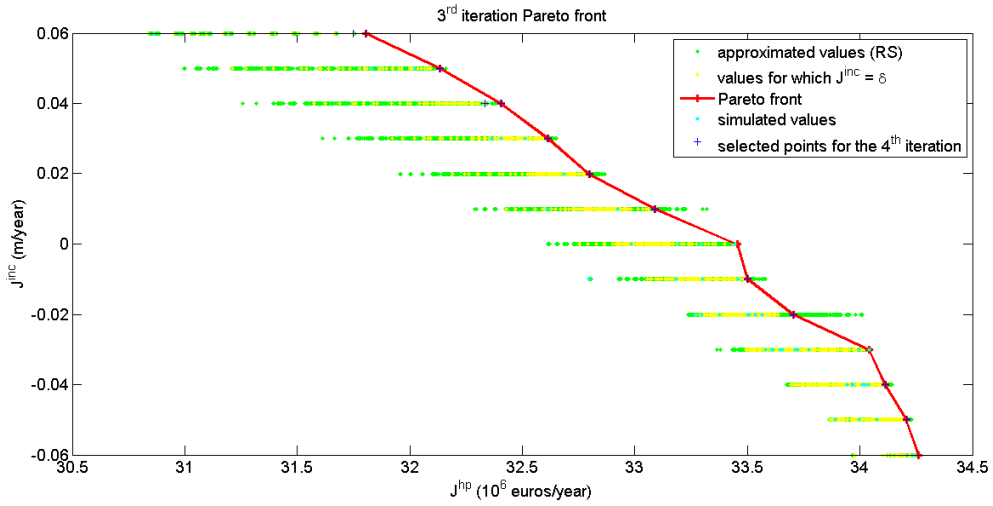

Figure 7.7: 3^{rd} iteration Pareto front (red line): the 22997 $\hat{J}^{INC}$ values generated by the RS approximation are rounded to two decimal places (green points), among these alternatives we identify the ones having $\hat{J}^{INC} = \delta$ (yellow points). The Pareto efficient alternatives are the ones maximizing $\hat{J}^{HP}$ (red points)

α	β	δ	$\hat{J}^{HP}$ (10^6€/y)	$\hat{J}^{INC}$ (m/10y)
1200	2000	0.06	31.80523902	0.06
2700	4900	-0.01	33.50170941	-0.01
1600	4900	0.02	32.7972892	0.02
1500	3600	0.03	32.61365461	0.03
4000	3000	-0.05	34.20672297	-0.05
3600	1900	-0.04	34.113985	-0.04
2900	2100	-0.02	33.70559786	-0.02
2000	4700	0.01	33.09083585	0.01
1200	3700	0.04	32.4047571	0.04
1400	2100	0.05	32.13524644	0.05
1200	1900	0.06	31.74710889	0.06
3700	4000	-0.04	34.04502888	-0.03

Table 7.18: Selected alternatives for the 4^{th} iteration (framework B)

α	β	δ	J^{HP} (10^6€/y)	J^{INC} (m/10y)
1200	2000	0.06	31.70435	0.05
2700	4900	-0.01	33.60701	-0.02
1600	4900	0.02	32.44710	0.01
4000	3000	-0.05	34.13809	-0.05
3600	1900	-0.04	34.11167	-0.05
2900	2100	-0.02	33.74931	-0.03
2000	4700	0.01	32.63766	-0.01
1200	3700	0.04	32.37246	0.04
1400	2100	0.05	31.99136	0.04
1200	1900	0.06	31.71904	0.06
3700	4000	-0.04	33.9543	-0.04
1500	3600	0.03	32.55059	0.03

Table 7.19: 4^{th} iteration model outcomes (framework B)

7.2.5 *Fourth iteration*

7.2.5.1 *Simulation runs*

The 12 previously selected interesting alternatives are simulated by means of the PB model. Results are shown in Table 7.19.

7.2.5.2 *Termination test*

The termination test is then performed (Table 7.20). Both average absolute differences resulted below the respective threshold which means the RS approximation procedure can be stopped at this iteration. We reached the target confidence rate of 94%.

7.2.5.3 *Response surface identification*

Once again for both indicators the RS is approximated using a RBF Multiquadratic interpolation which proved the best cross-validation performances (Table 7.21).

7.2.5.4 *Pareto front*

A new Pareto front (Figure 7.8) is identified from the last RS approximation.

7.2.6 *Results analysis*

Figures 7.9, 7.10, 7.11 and 7.12 show the Pareto front convergence over the four performed iterations. This is related to the convergence

	α	β	δ	ΔJ^{HP} (10^6€/y)	ΔJ^{INC} (m/10y)
	1200	2000	0.06	-0.100893021	-0.010045161
	2700	4900	-0.01	0.105299587	-0.005806452
	1600	4900	0.02	-0.350190201	-0.0136
	1500	3600	0.03	-0.063060605	-0.001135484
	4000	3000	-0.05	-0.068631968	-0.00343871
	3600	1900	-0.04	-0.002318996	-0.008729033
	2900	2100	-0.02	0.043715143	-0.009606452
	2000	4700	0.01	-0.453171847	-0.016316129
	1200	3700	0.04	-0.032300103	-0.0044
	1400	2100	0.05	-0.143886439	-0.011987097
	1200	1900	0.06	-0.028064891	-0.001374194
	3700	4000	-0.04	-0.090728882	-0.00736129
|**average**|				**0.12199**	**0.00782**

J	RANGE	λ (6% threshold)
$\hat{J}_{hp}$(10^6€/y)	3.4383	**0.206298**
$\hat{J}_{inc}$(m/10y)	0.13	**0.0078**

Table 7.20: 4^{th} iteration termination test (framework B)

Interpolator	J^{HP}	J^{INC}
Linear interpolator	$3.21 \cdot 10^{-}5$	0.004032255
RBF Gaussian	1526482.62	28326145.48
RBF Thin plate	0.239237605	1.838010512
RBF Cubic	10226.17547	145783.3393
RBF Multiquadratic	$\mathbf{1.48 \cdot 10^{-5}}$	**0.002545604**

Table 7.21: Cross validation results: mean errors for the 5 interpolation functions tested for the 4^{th} iteration (framework B)

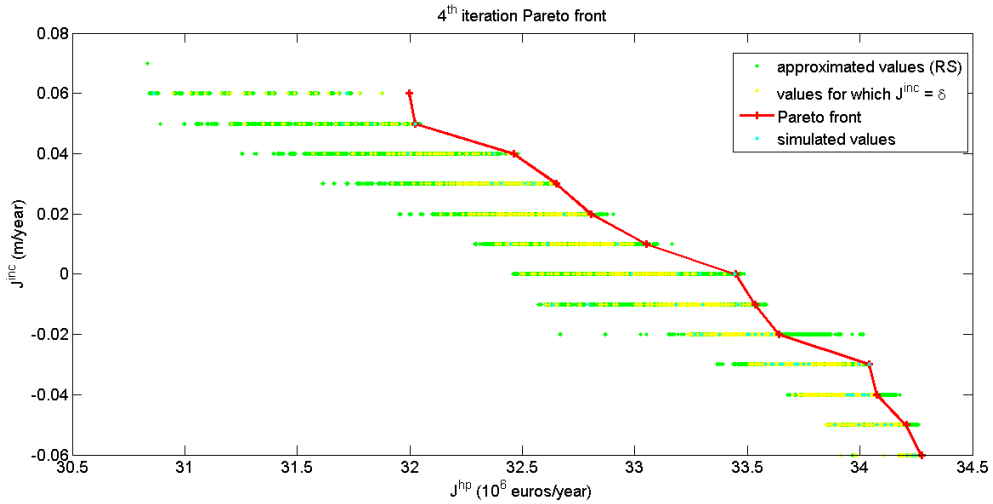

Figure 7.8: 4^{th} iteration Pareto front (red line): the 22997 $\hat{J}^{INC}$ values generated by the RS approximation are rounded to two decimal places (green points), among these alternatives we identify the ones having $\hat{J}^{INC} = \delta$ (yellow points). The Pareto efficient alternatives are the ones maximizing $\hat{J}^{HP}$ (red points).

of the RS approximations to the PB model RS proved by the termination tests.

The RS approximation is based on the training data set; which means the approximated RS will try to reproduce the system behavior observed in the simulations. As the training set increases the approximations reach a better confidence rate.

In particular the 1^{st} and 2^{nd} RS approximation did not cover the whole δ domain (from -0.06 to +0.06) since the training data sets were limited to certain J^{INC} values. This is mirrored by the respective Pareto fronts.

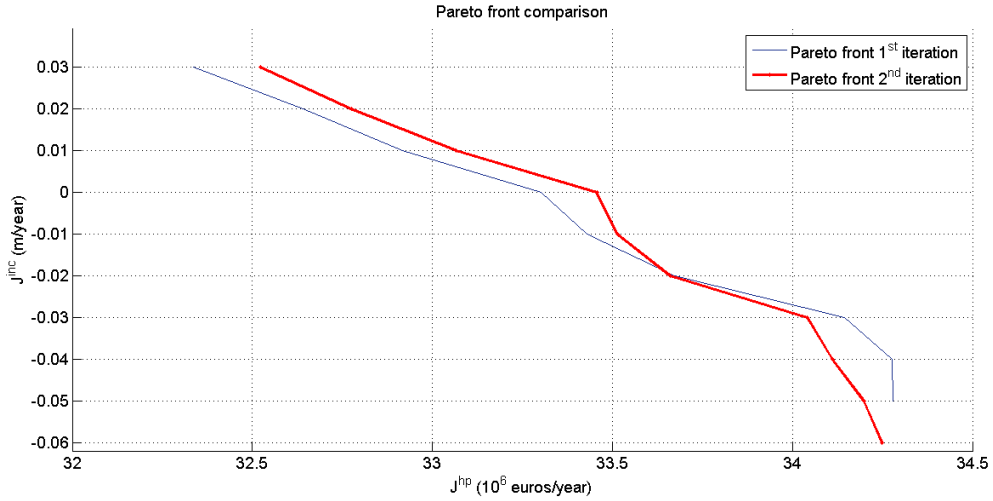

Figure 7.9: 1st and 2nd iteration Pareto fronts comparison

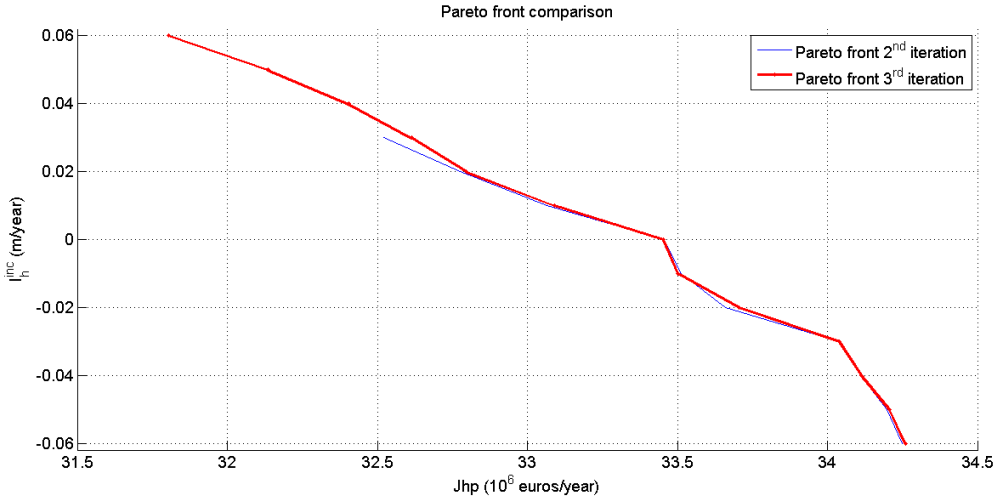

Figure 7.10: 2nd and 3rd iteration Pareto fronts comparison

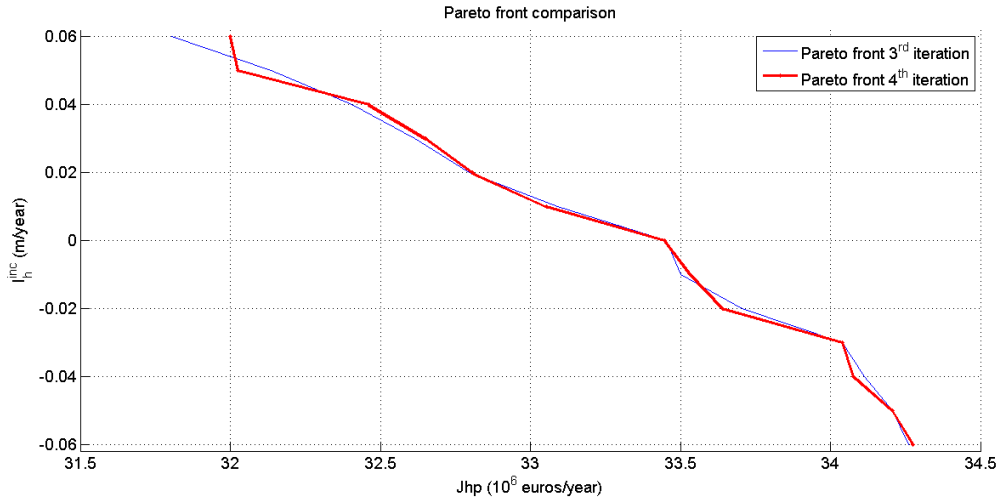

Figure 7.11: 3^{rd} and 4^{th} iteration Pareto fronts comparison

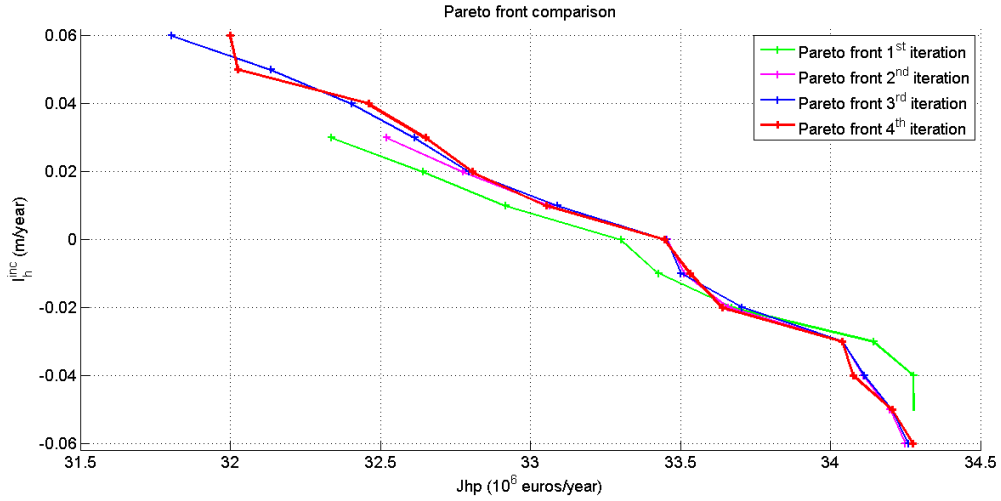

Figure 7.12: Pareto front convergence and comparison to the BAU alternative

8

CONCLUSIONS AND FURTHER RESEARCH

The goal of this study was to to investigate the possibility of re-operating HP plants in such a way to balance energy production and downstream riverbed incision.

Including riverbed incision abatement among the objectives when planning a dam control law turned out to be an effective method for contrasting the negative effects of HP operations on the river geomorphology without affecting too much the power company revenue.

In turn, the application of the RS method appeared to be a good approach for managing the limitations of combining together fluvial geomorphology complex behavior and optimal reservoir operation planning.

As a matter of fact from our case study results, presented in Chapter 7, it can be inferred that riverbed incision could both be put to an end (framework A and B) and turned into deposition (framework B) with a restrained decrease in HP production as a trade off.

Framework B outcomes, thus showing that it is possible to keep riverbed incision rate close to a wanted target, bring about many possibilities for river geomorphology rehabilitation: a combination of different alternatives performing geomorphic restoration at a first stage and conservation in a second phase could be considered.

The impressive growth of the number of large dams and interconnected reservoirs in developing countries which was observed in the last decades makes it necessary to develop effective control strategies in order to predict and contrast both direct and indirect effects of these systems on the river geomorphology

For this reason further research could consider the application of the present solution procedure to bigger and more complex systems which may be formed by several interconnected reservoirs destined to multiple purposes.

BIBLIOGRAPHY

[1] Adil Al Radif. "Integrated water resources management (IWRM): an approach to face the challenges of the next century and to avert future crises." In: *Desalination* 124.1 (1999), pp. 145–153.

[2] George EP Box and KB Wilson. "On the experimental attainment of optimum conditions." In: *Journal of the Royal Statistical Society. Series B (Methodological)* 13.1 (1951), pp. 1–45 (cit. on p. 21).

[3] S Anders Brandt. "Classification of geomorphological effects downstream of dams." In: *Catena* 40.4 (2000), pp. 375–401 (cit. on p. 15).

[4] Gary Brierley. "Geomorphology and River Management." In: () (cit. on p. 15).

[5] Gary Brierley and Kirstie Fryirs. *Geomorphology and river management: applications of the river styles framework*. Wiley-Blackwell, 2008.

[6] A Castelletti, AV Lotov, and R Soncini-Sessa. "Visualization-based multi-objective improvement of environmental decision-making using linearization of response surfaces." In: *Environmental Modelling & Software* 25.12 (2010), pp. 1552–1564 (cit. on p. 22).

[7] A Castelletti and R Soncini-Sessa. "A procedural approach to strengthening integration and participation in water resource planning." In: *Environmental Modelling & Software* 21.10 (2006), pp. 1455–1470 (cit. on p. 15).

[8] A Castelletti et al. "A general framework for Dynamic Emulation Modelling in environmental problems." In: *Environmental Modelling & Software* 34 (2012), pp. 5–18.

[9] A Castelletti et al. "A multiobjective response surface approach for improved water quality planning in lakes and reservoirs." In: *Water Resources Research* 46.6 (2010) (cit. on p. 22).

[10] A Castelletti et al. "Data-driven dynamic emulation modelling for the optimal management of environmental systems." In: *Environmental Modelling & Software* 34 (2012), pp. 30–43.

[11] A Castelletti et al. "Interactive response surface approaches using computationally intensive models for multiobjective planning of lake water quality remediation." In: *Water Resources Research* 47.9 (2011) (cit. on pp. 22, 23).

[12] A. Castelletti et al. "Planning infrastructural measures for controlling saltwater intrusion in a coastal aquifer by Global Interactive Response Surfaces: the Nauru island case study." In: *International Congress on Environmental Modelling and Software Managing Resources of a Limited Planet*. 2012.

[13] Andrea Castelletti, Francesca Pianosi, and Rodolfo Soncini-Sessa. "Integration, participation and optimal control in water resources planning and management." In: *Applied Mathematics and Computation* 206.1 (2008), pp. 21–33 (cit. on p. 15).

[14] Andrea Castelletti et al. "Dynamic Emulation Modelling of a 1D Hydrodynamic-Ecological Model: Tono Dam Case Study." In: *World Congress*. Vol. 18. 1. 2011, pp. 14170–14175.

[15] S.E. Darby and A Simon. *Incised River Channels: Processes, Forms, Engineering, and Management*. Wiley, 1999 (cit. on p. 15).

[16] Galileo Galilei. *Dialogue Concerning the Two Chief World Systems*. 1632 (cit. on p. 1).

[17] GE Grant, JC Schmidt, and SL Lewis. "A geological framework for interpreting downstream effects of dams on rivers." In: *Water Science and Application* 7 (2003), pp. 203–219 (cit. on pp. 7, 15).

[18] Harish Gupta, Shuh-Ji Kao, and Minhan Dai. "The role of mega dams in reducing sediment fluxes: A case study of large Asian rivers." In: *Journal of Hydrology* (2012) (cit. on pp. 5, 15).

[19] ICOLD, ed. *Dams and the world's water*. Paris, 2007 (cit. on p. 5).

[20] Jack PC Kleijnen. "Response surface methodology for constrained simulation optimization: An overview." In: *Simulation Modelling Practice and Theory* 16.1 (2008), pp. 50–64 (cit. on p. 22).

[21] G Mathias Kondolf. "Hungry water: effects of dams and gravel mining on river channels." In: *Environmental management* 21.4 (1997), pp. 533–551 (cit. on pp. 5, 7, 15).

[22] Yuanxu Ma et al. "Channel adjustments in response to the operation of large dams: The upper reach of the lower Yellow River." In: *Geomorphology* 147 (2012), pp. 35–48.

[23] Francis J Magilligan and Keith H Nislow. "Changes in hydrologic regime by dams." In: *Geomorphology* 71.1 (2005), pp. 61–78 (cit. on p. 6).

[24] MATLAB. *version R2013a*. Natick, Massachusetts: The MathWorks Inc., 2013 (cit. on p. 51).

[25] Matthew McCartney et al. "Living with dams: managing the environmental impacts." In: *Water Policy* 11.Supplement. 1 (2009), pp. 121–139 (cit. on pp. 8, 12, 13).

[26] Giuseppe Oldani et al. “Erosion control through an observational approach at Isola Serafini gate structure on the river Po, Italy.” In: () (cit. on pp. 12, 31).

[27] Sara Pavan. “Modello evolutivo monodimensionale per correnti a fondo mobile e brecce su rilevati in terra.” In: () (cit. on p. 35).

[28] G. E. Petts. *Impounded rivers*. Wiley, 1984 (cit. on pp. 5, 6).

[29] Geoffrey E Petts. “Long-term consequences of upstream impoundment.” In: *Environmental Conservation* 7.4 (1980), pp. 325–332 (cit. on pp. 5, 15).

[30] Geoffrey E Petts and Angela M Gurnell. “Dams and geomorphology: research progress and future directions.” In: *Geomorphology* 71.1 (2005), pp. 27–47 (cit. on pp. 5, 6, 15).

[31] Agenzia interregionale per il fiume Po. “Il progetto di sistemazione a corrente libera del Po tra Cremona e foce Mincio.” In: ().

[32] Agenzia Iterregionale per il fiume Po. *AIPo*. URL: http://www.agenziainterregionalepo.it/ (cit. on p. 29).

[33] Mary E Power, William E Dietrich, and Jacques C Finlay. “Dams and downstream aquatic biodiversity: potential food web consequences of hydrologic and geomorphic change.” In: *Environmental management* 20.6 (1996), pp. 887–895 (cit. on pp. 8, 15).

[34] Saman Razavi, Bryan A Tolson, and Donald H Burn. “Review of surrogate modeling in water resources.” In: *Water Resources Research* 48.7 (2012) (cit. on pp. 21, 22).

[35] M Rinaldi, B Wyżga, and N Surian. “Sediment mining in alluvial channels: physical effects and management perspectives.” In: *River Research and Applications* 21.7 (2005), pp. 805–828 (cit. on p. 15).

[36] Massimo Rinaldi. “La prospettiva geomorfologica e le applicazioni nella gestione degli alvei fluviali.” In: *Atti del convegno: Nuovi approcci per la comprensione dei processi fluviali e la gestione dei sedimenti. Applicazioni nel bacino del Magra* (2006), pp. 24–25 (cit. on p. 11).

[37] Paolo Ronco et al. “Morphological effects of damming on lower Zambezi River.” In: *Geomorphology* 115.1 (2010), pp. 43–55.

[38] G Rosatti et al. “L’uso di pennelli per la riduzione della barra forzata in prossimità del punto di inflessione tra due curve susseguenti: uno studio numerico relativo al Po.” In: () (cit. on p. 38).

[39] Schippa, Pavan, and Colonna. “The importance of mathematical modeling to support designing activities.” In: *River Flow 2006, Two Volume Set*. Ed. by João G . A . B . Leal Elsa C . T . L . Alves António H . Cardoso and Rui M . L . Ferreira. 2006. Chap. 216. River Po low water training.

[40] Leonardo Schippa and Sara Pavan. "Analytical treatment of source terms for complex channel geometry." In: *Journal of Hydraulic Research* 46.6 (2008), pp. 753–763.

[41] Leonardo Schippa and Sara Pavan. "Bed evolution numerical model for rapidly varying flow in natural streams." In: *Computers & Geosciences* 35.2 (2009), pp. 390–402 (cit. on p. 34).

[42] Rodolfo Soncini-Sessa, Enrico Weber, and Andrea Castelletti. *Integrated and participatory water resources management-theory*. Vol. 1. Elsevier Science, 2007 (cit. on p. 16).

[43] Donald F Specht. "A general regression neural network." In: *Neural Networks, IEEE Transactions on* 2.6 (1991), pp. 568–576.

[44] Nicola Surian and Massimo Rinaldi. "Morphological response to river engineering and management in alluvial channels in Italy." In: *Geomorphology* 50.4 (2003), pp. 307–326 (cit. on pp. 8, 9, 11).

[45] Nicola Surian et al. "Channel adjustments in northern and central Italy over the last 200 years." In: (2009) (cit. on p. 31).

[46] Yongyong Zhang et al. "Water quantity and quality optimization modeling of dams operation based on SWAT in Wenyu River Catchment, China." In: *Environmental monitoring and assessment* 173.1-4 (2011), pp. 409–430.

[47] Yongyong Zhang et al. "Water quantity and quality simulation by improved SWAT in highly regulated Huai River Basin of China." In: *Stochastic Environmental Research and Risk Assessment* 27.1 (2013), pp. 11–27 (cit. on p. 23).